Chem Soc Rev

A multicompoment molecular approach to artificial photosynthesis

Journal:	*Chemical Society Reviews*
Manuscript ID	CS-TRV-10-2015-000774.R1
Article Type:	Review Article
Date Submitted by the Author:	11-Dec-2015
Complete List of Authors:	Rudolf, Marc; University of Erlangen-Nűrnberg, Department of Chemistry and Pharmacy Kirner, Sabrina; Friedrich-Alexander-Universitat Erlangen-Nurnberg, Department of Chemistry Guldi, Dirk; Friedrich-Alexander-Universitaet Erlangen-Nuernberg, Department of Chemistry and Pharmacy

Journal Name

ARTICLE

A multicomponent molecular approach to artificial photosynthesis - the role of fullerenes and endohedral metallofullerenes

Received 00th January 20xx,
Accepted 00th January 20xx

DOI: 10.1039/x0xx00000x

www.rsc.org/

M. Rudolf,[a†] S. V. Kirner[a†] and D. M. Guldi[a]

In this review article, we highlight recent advances in the field of solar energy conversion at a molecular level. We focus mainly on investigations regarding fullerenes as well as endohedral metallofullerenes in energy and/or electron donor-acceptor conjugates, hybrids, and arrays, but will also discuss several more advanced systems. Hereby, the mimicry of the fundamental processes occurring in natural photosynthesis, namely light harvesting (LH), energy transfer (EnT), reductive/oxidative electron transfer (ET), and catalysis (CAT), which serve as a blue print for the rational design of artificial photosynthetic systems, stand at the focalpoint. Importantly, the key processes in photosynthesis, that is, LH, EnT, ET, and CAT, define the structure of this review with the only further differentiation in terms of covalent and non-covalent systems. Fullerenes as well as endohedral metallofullerenes are chosen by virtue of their small reorganization energies in electron transfer processes, on one hand, and their exceptional redox behaviour, on the other hand.

1. Introduction

Natural photosynthesis is a highly sophisticated process, where solar energy is converted into chemical energy in the form of chemical bonds in organic molecules. In fact, photosynthesis generates organic molecules that are the building blocks of all living organisms. Also fossil fuels, such as oil, natural gas, and coal originate from photosynthetic activity. They formed millions of years ago, when large quantities of dead organisms were buried underneath sedimentary rock and subjected to intense heat and pressure. The success of natural photosynthesis is based on the fact that sunlight, water, and carbon dioxide, are available in abandon quantities. Still, the evolution of plants was governed by survival and successful reproduction rather than by maximum efficiency of biomass production. Thus, the overall solar energy to dry matter conversion yield is rather moderate with yields seldomly exceeding 1%.[1] Despite the aforementioned, natural photosynthesis, especially the early events, that is, light harvesting (LH), energy transfer (EnT, ), and electron transfer (ET,), proceed with unit quantum efficiencies. It is fair to say that the light harvesting pigments and the electron transport chain provide a blue print for artificial photosynthetic model systems. Solar energy is absorbed, for example, by chlorophylls, carotenoids, and other pigments and is consequently funnelled to the photosynthetic reaction centre, where the initial charge separation takes place. At the heart of the photosynthetic reaction centre is a pair of chlorophylls, which are in close van-der-Waals distance. Once photoexcited either by direct light absorption or by transduction of singlet excited state energy from the antenna systems, it donates an electron to a neighbouring pheophytin - Fig. 1. Noteworthy, electron transfer processes over large distances tend to be rather slow and, thus, to be non-competitive with respect to energy dissipating reactions. To circumvent this inherent problem, photosynthetic organisms have developed sequences of short-range electron transfer events, which finally generate long lived transmembrane charge-separated states. The initial electron transfer from the special pair to a neighbouring pheophytin takes about 3 ps. Within a few hundred picoseconds the reduced pheophytin transfers its extra electron to an electron accepting plastoquinone Q. Plastoquinone accepts, however, two electrons and two protons to yield its plastoquinol QH_2 form in the micro- to millisecond time regime according to its redox state. This happens prior its diffusion from the reaction centre to the cytochrome b_6f complex. The latter together with plastocyanine assist in releasing energy to convert adenosine diphosphate (ADP) into adenosine triphosphate (ATP). ATP is required, along with dihydronicotinamide adenine dinucleotide phosphate (NADPH), to convert CO_2 into energy rich carbon hydrates. The oxidized special pair is re-reduced to its neutral form via a redox active tyrosine, which channels electrons from the oxygen evolving complex (CAT, ). Thus, the oxidizing potential to facilitate water splitting in the Mn_4Ca-cluster of the oxygen evolving complex – Fig. 1 – is provided.[1-10]

[a] Department of Chemistry and Pharmacy & Interdisciplinary Center for Molecular Materials (ICMM), Friedrich-Alexander-University Erlangen-Nuremberg, Egerlandstr. 3, 91058 Erlangen, Germany. E-mail: dirk.guldi@fau.de.
† These authors contributed equally to this work.

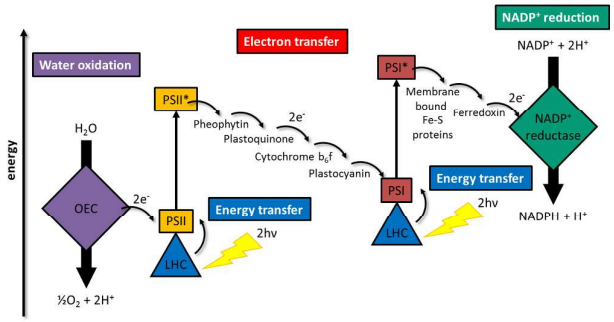

Fig. 1: Schematic representation of the early events in natural photosynthesis with light absorbing units (LHC) of photosystem I (PSI) and photosystem II (PSII), the electron transport chain with its principal components, on one hand, the oxygen evolving complex (OEC), and, on the other hand, the $NADP^+$ reductase as catalytic centers (CAT).[9]

1.1. From natural to artificial photosynthesis

The key concepts, which are typically borrowed from natural photosynthesis in order to achieve efficient artificial solar to chemical energy conversion are light harvesting, energy transfer, and electron transfer.

Light harvesting is important and requires to be optimized in artificial photosynthesis – the more light is harnessed the more charges are likely be separated and consequently be utilized. In this regard, particular emphasis has been placed on extending the visible light absorption features of chromophores into the near-infrared region, since the solar spectrum spans over all these regions.[10-14] A rather elegant but, yet, simple approach involves electron donors or acceptors with high extinction coefficients in the visible part of the solar spectrum. The complexity is kept at a comparably simple level. To increase the absorption characteristics in the long wavelength region a probate means is the extension of the delocalized π-system. This goes, however, along with changes in the electronic properties – most notable are the HOMO and LUMO levels and redox potentials. Alternatively, light harvesting, energy transfer, and electron transfer are synchronized in a single system similar to what is known in natural photosynthesis. For example, to an electron donor-acceptor couple at least one light harvester, which transduces excited-state energy to either the electron donor or acceptor, is linked. In the latter, charge separation takes place. In such a case, neither the electron donor nor the electron acceptor necessarily need to feature strong absorptions. Finally, panchromatic light harvesting, that is, the complementary matching of the absorption features of the different chromophores, should be considered.

In terms of EnT, different mechanisms are known. Förster resonant energy transfer (FRET) is a non-radiative EnT. Here, the energy is transferred between energy donor and acceptor primarily via dipole-dipole Coulomb interactions. Its rate (k) falls off with the sixth power of the distance (eq. 1), [10, 11] where k_{EnT} is the first-order rate constant for energy transfer from the energy donor to the acceptor, k_f is the rate constant for fluorescence of the energy donor, R is the distance between energy donor and acceptor, and R_0 is the distance, at which the energy transfer proceeds with 50% efficiency.

$$k_{EnT(Förster)} = k_f\,(R_0/R)^6 \qquad (1)$$

Energy conversion demands for an efficient FRET that the energy donor's emission overlaps with the energy acceptor's absorption. This overlap criterion, however, should not be mistaken in the way that emission and/or absorption of a photon occur. As a matter of fact, FRET is a strictly non-radiative process. FRET is known to be operative even at long distances in contrast to the exchange energy transfer – vide infra – owing to the fact that the nature of the dipole-dipole Coulomb coupling does not require direct overlap of the wave functions.

The exchange or so called Dexter EnT requires an overlap of electron density. If this is fulfilled, electrons are exchanged freely between two different molecular building blocks. Therefore, this mechanism is also called exchange energy transfer. While actual contact is not required close proximity in the range of 1 - 1.5 nm is. The distance dependence of the energy transfer rate by the exchange mechanism infers an exponential fall off (eq. 2),[10, 11] where J is the spectral overlap integral and L is the effective orbital radius.

$$k_{EnT(Dexter)} \propto J\,exp(-2R/L) \qquad (2)$$

The exchange mechanism requires the simultaneous transfer of electrons between the energy donor and acceptor. The acceptor remains uncharged throughout the exchange process. Thereby, the spin conversion rules are obeyed. Triplet-triplet energy transfer processes proceed exclusively via the Dexter exchange energy transfer. For singlet-triplet energy transfer the spectral overlap is very small and, as a consequence, the Förster mechanism dominates. At small energy donor-acceptor distances the Förster and Dexter mechanisms compete for the singlet-singlet energy transfer.[14, 15]

When turning to electron transfer, the correlation between its rate and the thermodynamic parameters is well-described by the Marcus theory for electron transfer.[16] The latter provides basic principles, which allow the quantitative interpretation of electron transfer rates. The rate constant for non-adiabatic intramolecular electron transfer (k_{ET}) is given by eq. 3, where h is the Planck constant, λ the total reorganization energy, T the Temperature, V the electronic coupling matrix element, and ΔG^0_{ET} the standard free energy change upon electron transfer.

$$k_{ET} = \left(\frac{4\,\pi^3}{h^2\,\lambda\,k_B\,T}\right)^{\frac{1}{2}} V^2\ exp\left[-\frac{(\Delta G^0_{ET}+\lambda)^2}{4\,\lambda\,k_B\,T}\right] \qquad (3)$$

The graphic representation of eq. 3 in the form of $-\Delta G^0_{ET}$ versus $\log k_{ET}$ gives a parabolic dependence for the electron transfer rates – Fig. 2. Hereby, the importance and the nature of both the electronic coupling V and the reorganization energy λ on the electron transfer dynamics is highlighted. A rational design implies small reorganization energies for the electron transfer partners, that is, electron donor and acceptor. The immediate consequences of either a small or a large reorganization energy are illustrated in Fig. 2.

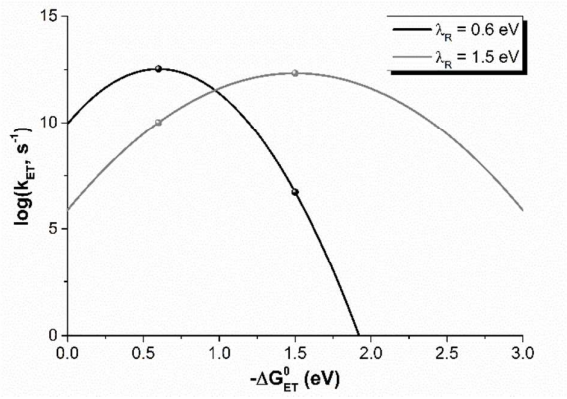

Fig. 2: Thermodynamic driving force dependence of the electron transfer rates, as $\log(k_{ET})$, for two different reorganization energies (λ_R = 0.6 or 1.5 eV).

At a comparable electronic coupling (e.g. 100 cm^{-1}) and similar driving forces for charge separation and charge recombination the magnitude of λ has a profound impact on the electron transfer dynamics. For a small λ, the charge separation, on one hand, proceeds at/or close to the top region of the Marcus parabola, resulting in an ultrafast electron transfer. The charge recombination, on the other hand, is pushed far into the inverted region of the Marcus parabola and, thus, effectively slows down the energy-wasting back electron transfer. In contrast, a large λ leads to slower charge separation, which consequently diminishes the efficiency of charge separation. More importantly, a large λ accelerates the charge recombination leading to short lived radical ion pairs.

The total reorganization energy is composed of a solvational (λ_s) and a vibrational (λ_i) term (eq. 4).

$$\lambda = \lambda_s + \lambda_i \quad (4)$$

An important requirement for small internal reorganization energies in electron donor-acceptor systems is the use of molecular building blocks of high rigidity and, in turn, low λ_i. This consideration is equally applicable to the electron donor as well as to the electron acceptor. The use of solvents of different polarity helps to fine-tune the overall reorganization energy by changing λ_S. Fullerenes, in general, and endohedral metallofullerenes (EMF), in particular, exhibit remarkably low reorganization energies in electron transfer processes. Such an intrinsic property complemented by a number of outstanding redox properties – ranging from strong electron accepting ability for empty fullerenes to strong electron donating properties and even a highly amphotheric electrochemical behaviour of EMFs – renders them ideal candidates as electron acceptors as well as electron donors for artificial photosynthetic mimics.[17-25] Not surprising, ultrafast charge separation together with very slow charge recombination lead in fullerene based electron donor–acceptor systems to unprecedentedly long-lived radical ion-pair states with high quantum efficiencies – vide infra.[4, 26-28]

Next to influences stemming from reorganization energies, the intervening medium between electron donors and acceptors governs the electronic coupling and, thus, the electron transfer dynamics. In particular, the top region of the Marcus parabola is modulated by the magnitude of electronic coupling V. In principal, the electronic coupling depends on the involved states of electron donors and acceptors and their respective distances (R_{DA}). Its magnitude decreases exponentially as a function of distance according to eq. 5.[29]

$$V^2 = V_0^2 \, exp(-\beta \, R_{DA}) \quad (5)$$

Taken the aforementioned into concert, the Marcus theory of electron transfer is a valuable tool to design efficient artificial photosynthetic model systems. For the realization of fast charge separation together with slow charge recombination, small λ_i of the respective molecular building blocks in electron transfer reactions is a must. In addition, the solvent/environment should be apolar to keep λ_s low. Last but not least, the nature of the spacers and the distance between electron donors and acceptors have tremendous effects on the electronic communication and, therefore, the electron transfer rate.

We have chosen a structure for our review, which is an adaption of the key processes in natural photosynthesis starting with LH and EnT. This is followed by reductive as well as oxidative ET and rounded off by CAT. Major emphasis is placed on fullerenes and endohedral metallofullerenes (EMF) as they were combined with a myriad of chromophores and other building blocks to mimic natural photosynthesis. Considering that both covalently linked conjugates and non-covalently associated hybrids play an important, but different role we have subdivided each chapter.

2. Artificial photosynthesis

2.1. LH and EnT – see Fig. 1

One of the essential processes in natural photosynthesis is light harvesting. In nature, this is accomplished by chromophores such as chlorophyll a and b, as well as carotenoids. For artificial photosynthesis various chromophores that absorb light in the visible region of the solar spectrum have been studied, amongst them are tetra-pyrrolic macrocycles – porphyrins (Por), phthalocyanines (Pc) or chlorines – carotenoids, subphthalocyanines, boron dipyrromethene (BODIPY), perylenebisimides (PDI), tetrathiafulvalenes (TTF), and π-extended tetrathiafulvalene (exTTF). In analogy to natural photosynthesis any of the aforementioned chromophores can harvest and transfer solar energy to a reaction center, where charge separation takes place.

2.1.1. Covalently linked energy donor-acceptor conjugates

Various conjugates comprised of Pors and Pcs have been examined,[30] owing to the fact that they feature complimentary absorption throughout the visible range of the solar spectrum. LH and EnT properties strongly depend, on one hand, on the way the two different tetrapyrrolic marcocycles are linked and, on the other hand, on the fine tuning of their electronic features by introducing different peripheral substituents or metal centers as well as on the molecular topology of the ensemble. In general, Por-Pc systems are known to efficiently transfer singlet excited state energy from Pors to Pcs, since the long-wavelength Q-band absorption of Pcs overlaps with the short-wavelength fluorescence of Pors. Fig. 3 shows a couple of Por-Pc conjugates that undergo EnT with rate constants in the range of 10^{10}-10^{11} s^{-1}.[31, 32]

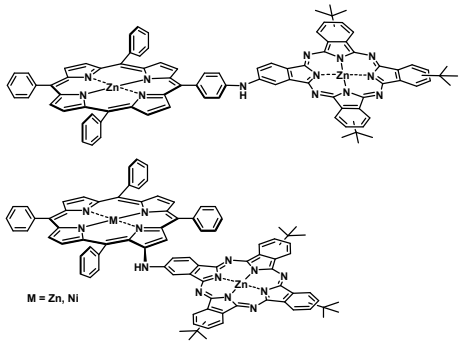

Fig. 3 Structures of porphyrin/phthalocyanine – ZnPc-ZnPor – based energy donor-acceptor conjugates.[31, 32]

Similar rate constants for EnT were observed in a pentad comprised of four RuPcs and one H_2Por, which bears four phenylimidazoles at its meso position, to which Ru is coordinated – Fig. 4.[33]

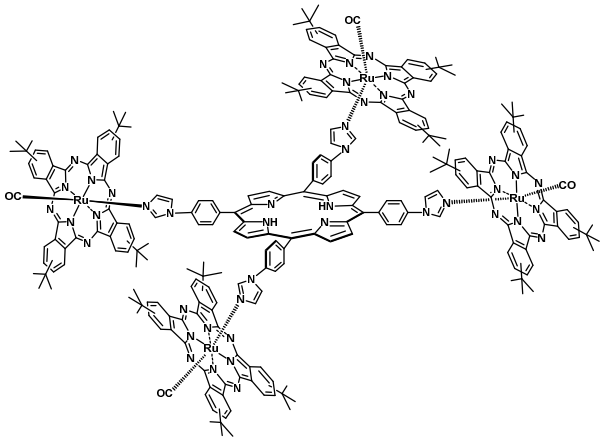

Fig. 4 Structure of a porphyrin/phthalocyanine – H_2P-(Ru(CO)Pc)$_4$ – based energy donor-acceptor conjugate.[33]

In complementary studies BODIPY was employed in combination with, for instance, Por in order to assure efficient light harvesting and EnT. Excitation, for example, of BODIPY at 500 nm in a cyanuric chloride linked BODIPY-ZnPor conjugate – Fig. 5 – gives rise to EnT with rate constants of 2-3 x 10^{10} s^{-1}.[34]

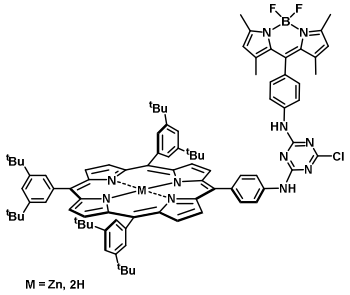

Fig. 5 Structure of a boron dipyrromethene/porphyrin – BODIPY-ZnPor – based energy donor-acceptor conjugate.[34]

2.1.2 Non-covalently linked energy donor-acceptor hybrids

In a supramolecular approach, two ZnPcs were assembled with a PDI via highly directional triple hydrogen bonding – Fig. 6 – which guarantees light harvesting throughout the visible range. Here, energy is transferred from the PDI to the Pc via FRET with a rate constant of 3.3 x 10^8 s^{-1}.[35]

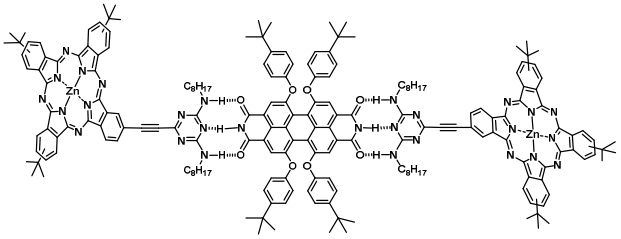

Fig. 6 Structure of a phthalocyanine/perylene – ZnPc/PDI – based energy donor-acceptor hybrid.[35]

2.2 Reductive ET – see Fig. 1

2.2.1. Covalently linked electron donor-acceptor conjugates

Another key step in natural photosynthesis is ET. It is mimicked by combining electron donating with accepting building blocks. To this end, the previously mentioned chromophores as well as ferrocene (Fc) and anilines, which easily donate electrons, and fullerenes were considered. Owing to the ability of their rigid structure to accept up to six electrons empty fullerenes such as C_{60}, C_{70}, C_{76}, etc. typically function as electron acceptors.[36] This has changed with the advent of endohedral metallofullerenes (EMF), which exhibit amphoteric redox properties, that is, serving as electron donor or acceptor.

2.2.1.1. Fullerenes and endohedral metallofullerenes in their excited states

To guarantee an efficient electron transfer the necessity arises to select suitable electron donors and combine them with fullerenes. In terms of photosynthetic reaction mimics, they need to feature the ability to efficiently harvest light and to match the redox requirements of C_{60} and/or EMFs. In the following, several examples of C_{60} in ET reactions are highlighted.

Diverse electron donating entities such as aniline,[37] Fc[38, 39] or TTF[40-42] have been covalently linked to C_{60} and investigated with respect to their ET properties. Nevertheless, the largest number of electron donor-acceptor conjugates is based either on Pors[43-47] (ZnPor/H_2Por) or Pcs[48-52] (ZnPc/H_2Pc), since they guarantee efficient light harvesting across the visible range of the spectrum.

In general, the nature of the spacer between the electron donor and acceptor is crucial for generating long-lived radical ion pairs. When considering, for example, the Fc-C_{60} conjugates[39] shown in Fig. 7, the role of the spacer becomes evident. In all of the four conjugates photoinduced ET occurs, but different lifetimes of the radical ion pairs point to different ET mechanisms. In those conjugates, where rigid unsaturated bridges (Fig. 7 top) are used, a through-bond ET takes place and fast charge recombination prevents sufficient stabilization of the radical ion pair. In contrast, in the conjugates with flexible linkers (Fig. 7 bottom) a transient intramolecular exciplex is formed yielding long lived radical ion pair states, which recombine with rate constants in the order of 10^5 s^{-1} in benzonitrile.

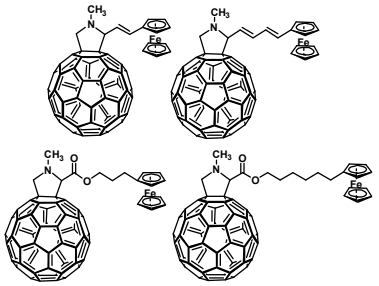

Fig. 7 Structures of ferrocene/fullerene – Fc-C_{60} – based electron donor-acceptor conjugates.[38, 39]

Fc-$Sc_3N@I_h$-C_{80}, a covalently linked electron donor-acceptor conjugate that comprises a ferrocene as electron donor and $Sc_3N@I_h$-C_{80} as electron acceptor, is one of the early milestones in the work on EMFs as integrative components in electron donor-acceptor systems – Fig. 8.[53-55]

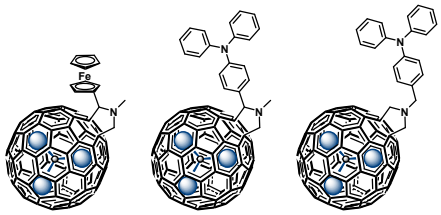

Fig. 8 Structures of ferrocene/endohedral metallofullerene – Fc-$Sc_3N@I_h$-C_{80} (left) – and triphenylamine/endohedral metallofullerene – TPA-$Sc_3N@I_h$-C_{80} (middle and right) – based electron donor-acceptor conjugates.[53, 54, 56]

Evidence for photoinduced formation of the $(Fc)^{\bullet+}$-$(Sc_3N@I_h\text{-}C_{80})^{\bullet-}$ radical ion pair state stems from the close resemblance of the near-infrared part of the transient-absorption measurements with the radiolytically and spectroelectrochemically generated spectrum of the one-electron reduced $Sc_3N@I_h$-C_{80} radical anion. Therefore, it was evident that ET from the $Sc_3N@I_h$-C_{80} singlet excited state (1.75 eV) results in the $(Fc)^{\bullet+}$-$(Sc_3N@I_h\text{-}C_{80})^{\bullet-}$ radical ion pair state (1.29 eV), which was concluded to be metastable. The decay of the latter was monitored with rate constants of 7.8 x 10^9 s^{-1} in carbon disulfide and 1.1 x 10^{10} s^{-1} in ortho-dichlorobenzene. Remarkably, a significant stabilization of the radical ion pair state is observed when compared to a similar Fc-C_{60} conjugate. The corresponding decays proceed with rate constants as high as 2.2 x 10^{10} s^{-1} in carbon disulfide, 2.0 x 10^{10} s^{-1} in THF, and 3.7 x 10^{10} s^{-1} in benzonitrile.

Next, two electron donor-acceptor conjugates comprising triphenylamine and $Sc_3N@I_h$-C_{80} were investigated.[56] The isomeric TPA-[5,6]-$Sc_3N@I_h$-C_{80}s differ in their substitution pattern, namely N-substituted versus 2-substituted pyrrolidine as shown in Fig. 8. In toluene and carbon disulfide, however, the radical ion pair states with energy values of 1.9 and 2.0 eV, respectively, would be thermodynamically uphill for the singlet excited state of $Sc_3N@I_h$-C_{80} (1.5 eV). In THF and benzonitrile the radical ion pair state energies were estimated to be 1.42 eV and 1.22 eV, respectively. In fact, the formation of the $(TPA)^{\bullet+}$-$(Sc_3N@I_h\text{-}C_{80})^{\bullet-}$ radical ion pair state was confirmed in polar solvents such as THF with time constants for ET of 3.4 x 10^{10} s^{-1} for the 2-substituted pyrrolidine conjugate. The corresponding charge recombination proceeds with rate constants of 1.7 x 10^9 and 4.5 x 10^8 s^{-1} in THF and benzonitrile, respectively. Increasing the electron donor acceptor separation, which was accomplished by linking TPA to the nitrogen rather than to the carbon of the pyrrolidine ring had a profound impact on the electron transfer dynamics. In particular, a larger donor-acceptor separation in TPA-$Sc_3N@I_h$-C_{80} leads to a notable slow down. In particular, forward ET proceeds with a time constant of 3.4 x 10^{10} s^{-1} in THF and back ET with <3.3 x 10^8 s^{-1} in benzonitrile. Notably, a comparison with the analogous TPA-C_{60} conjugates revealed distinct differences. Whereas the forward ET is just slightly slowed down, a notable slow-down of the back ET was found. For instance, rate constants for charge separation and charge recombination were 7.6 x 10^{10} and 8.0 x 10^9 s^{-1}, respectively, for the C-substituted TPA-C_{60} conjugate in THF. Overall, a relationship between rate constant versus solvent polarity was noted that suggests dynamics in the normal region of the Marcus parabola, where the rate constants increase with increasing thermodynamic driving force. For charge separation, reduced singlet excited state energies for $Sc_3N@I_h$-C_{80} (1.5 eV), compared to C_{60} (1.8 eV), are nearly compensated by lower radical ion pair state energies. In fact, the $(TPA)^{\bullet+}$-$(C_{60})^{\bullet-}$ radical ion pair has an energy of 1.67 eV in THF and 1.45 in benzonitrile. In this light, the charge recombination of $(TPA)^{\bullet+}$-$(Sc_3N@I_h\text{-}C_{80})^{\bullet-}$ is stabilized relative to $(TPA)^{\bullet+}$-$(C_{60})^{\bullet-}$.

In the context of stable electron donor acceptor conjugates involving an exTTF electron donor and a series of empty fullerenes, that is, C_{60}, and two EMFs, that is, the open-shell La@C_{2v}-C_{82} and the closed-shell $La_2@I_h$-C_{80} have been studied. In this context, the impact that different metallofullerenes exert on the excited state energies, radical ion pair state energies, and, consequently, on the electron transfer dynamics relative to C_{60} is of importance.[57] As evidenced by absorption spectroscopy and electrochemical measurements only weak electronic interactions were observed in the ground state despite the relatively close proximity between exTTF and fullerenes/EMFs. C_{60}, La@C_{2v}-C_{82}, and $La_2@I_h$-C_{80} are all versatile electron acceptors with first reduction potentials of -1.06, -0.38, and -0.45 V, respectively. When these reduction potentials and the exTTF centered oxidation is considered, radical ion pair state energies of 1.12 (exTTF-C_{60}), 0.43 (exTTF-La@C_{2v}-C_{82}), and 0.46 eV (exTTF-$La_2@I_h$-C_{80}) can be derived. Interestingly, both the exTTF singlet excited state (2.7 eV) as well as the fullerene singlet excited state (1.8 eV) and EMF singlet excited states (0.88 and 1.4 eV) are able to drive a fast ET from the electron donating exTTF to the electron accepting fullerenes to yield $(exTTF)^{\bullet+}$-$(C_{60})^{\bullet-}$, $(exTTF)^{\bullet+}$-$(La@C_{2v}\text{-}C_{82})^{\bullet-}$, or $(exTTF)^{\bullet+}$-$(La_2@I_h\text{-}C_{80})^{\bullet-}$. Photophysical assays reveal time constants for charge separation on the order of 10^{10} - 10^{11} s^{-1}. Charge recombination reinstates the singlet ground states and is slowed down at least two orders of magnitude and up to 4.9 x 10^6 s^{-1} for exTTF-C_{60} in polar benzonitrile. A large reorganization energy of at least 1.1 eV for the oxidation of exTTF rationalized by large structural changes forces the charge recombination into the normal region of the Marcus parabola. In other words, more polar solvents are desirable to stabilize the radical ion pair states.

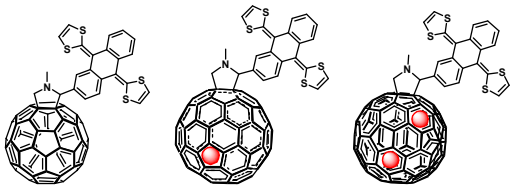

Fig. 9 Structures of π-extended tetrathiafulvalene/fullerene – ex-TTF-C_{60} (left) – and π-extended tetrathiafulvalene/endohedral metallofullerene – exTTF-La@C_{2v}-C_{82} (center) and exTTF-La_2@I_h-C_{80} (right) – based electron donor-acceptor conjugates.[57]

In comparison to natural photosynthesis lifetimes of several microseconds are fairly short. A system that overcomes this limit, despite of close proximity between electron donor and acceptor, is a zinc chlorin-C_{60} conjugate – Fig. 10 – with a radical ion pair state that decays with a rate constant of 8.3 x 10^{-3} s^{-1} at -150 °C.[58] Longer electron donor-acceptor separations are, however, required to further elongate the lifetimes.

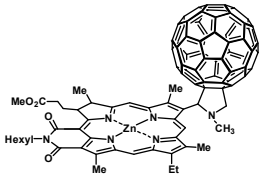

Fig. 10 Structure of a zinc chlorin/fullerene – ZnChlorin-C_{60} – based electron donor-acceptor conjugate.[58]

Different is the approach based on a conjugate, in which H_2Por was linked to La@C_{2v}-C_{82} – Fig. 11. In the excited state, H_2Por-La@C_{2v}-C_{82} gives rise to nearly quantitative quenching of the H_2Por fluorescence, which suggests efficient intramolecular EnT/ET events.[59, 60] Importantly, the calculated SOMO and LUMO are mainly localized on La@C_{2v}-C_{82}, while the HOMO is centered on H_2Por, in close agreement with electrochemical investigations.

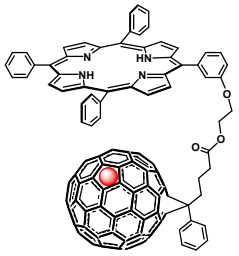

Fig. 11 Structure of a porphyrin/endohedral metallofullerene - H_2Por-La@C_{2v}-C_{82} – based electron donor-acceptor conjugate.[59, 60]

Likewise, 1,3-dipolar cycloaddition reaction of a corrole-based precursor with Sc_3N@I_h-C_{80} lead to Corrole-Sc_3N@I_h-C_{80}.[61] In the electronic ground state, absorption spectra suggest sizeable electronic communications between the electron donating corrole and the electron accepting EMF. Photophysical assays probed the electronically excited state. Directly after photoexcitation the initially populated singlet excited state of corrole decays ultrashort with rate constants of 1.7 x 10^{11} s^{-1} in toluene, 3.7 x 10^{11} s^{-1} in THF and 1.9 x 10^{11} s^{-1} in benzonitrile to yield the energetically low lying radical ion pair state (1.37 eV) consisting of the one-electron-reduced Sc_3N@I_h-C_{80} and of the one-electron-oxidized corrole, namely, $(corrole)^{\bullet+}$-$(Sc_3N@I_h\text{-}C_{80})^{\bullet-}$. From a global analysis, the rate constants for back ET were determined in toluene, THF, and benzonitrile as 3.7 x 10^{10}, 7.1 x 10^{11}, and 7.7 x 10^{11} s^{-1}, respectively.

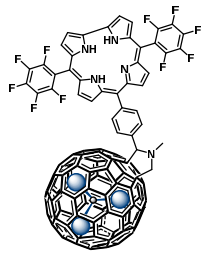

Fig. 12 Structure of a corrole/endohedral metallofullerene – corrole-Sc_3N@I_h-C_{80} – based electron donor-acceptor conjugate.[61]

To overcome distances of more than 20 Å, alternative concepts are needed, since long distance ET is a nonadiabatic process. Its rate is determined by a combination of weakly distance-dependent incoherent transport events and strongly distance-dependent tunnelling. The latter obeys a superexchange mechanism, in which the bridge orbitals do not contain any charges, but function solely as a coupling medium. In contrast, during incoherent ET intermediate states are formed that couple to internal nuclear motions of the bridge as well as the surrounding medium. Oligomers such, for instance *para*-phenylenevinylene[62] (oPPV), *para*-phenyleneethynylene[63] (oPPE), and fluorene[64] (oFL) – Fig. 13 – were proven to be suitable bridges for long distance ET. The gradual elongation of electron donor-acceptor distance, starting from ZnPor-C_{60} and implementing subsequently three and five oPPVs, results only in marginal changes in terms of radical ion pair state lifetimes. Even at electron donor-acceptor separations of 40 Å, electron donor-acceptor couplings of ~2.0 cm^{-1} were determined, due to, a low attenuation factor of 0.03 ± 0.005 $Å^{-1}$.

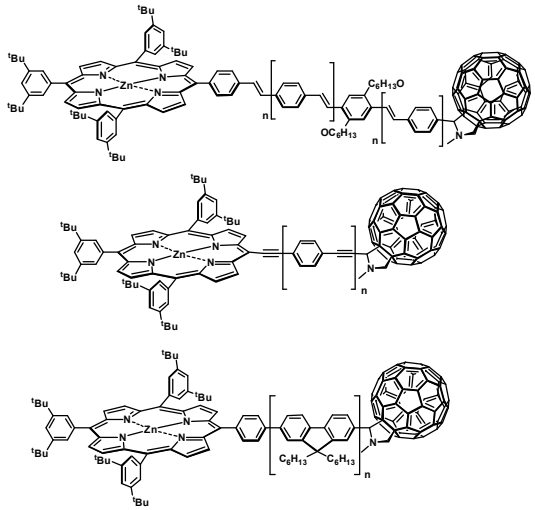

Fig. 13 Structures of porphyrin/fullerene – ZnPor-oPPV$_n$-C_{60} (top), ZnPor-oPPE$_n$-C_{60} (middle), and ZnPor-oFl$_n$-C_{60} (bottom) – based electron donor-acceptor conjugates.[62-64]

In complementary work, long-range ET events between ZnPor, as electron donor, and Sc_3N@I_h-C_{80}, as electron acceptor were investigated – Fig. 14.[65] It was shown that ET reactions are possible over center-to-center distances of up to 45 Å. The $(ZnPor)^{\bullet+}$-$(Sc_3N@I_h\text{-}C_{80})^{\bullet-}$ radical ion pair states – with driving forces of about 0.63 eV –

build up over the course of 6.7 x 10^8 s^{-1} and are persistent on femto, pico, and nanoseconds time-scales. As a matter a fact, kinetic analyses revealed rate constants of 1.0 x 10^6 s^{-1} for ZnPor-$Sc_3N@I_h$-C_{80} (I) and 8.3 x 10^5 s^{-1} for ZnPor-$Sc_3N@I_h$-C_{80} (II) in strictly oxygen free THF as well as 3.1 x 10^5 and 3.9 x 10^5 s^{-1} in benzonitrile at electron donor acceptor distances of 33 and 45 Å, respectively. Due to an electron donor-acceptor separation of 33 Å and the cathodically shifted reduction of $Sc_3N@I_h$-C_{80} relative to C_{60} charge recombination is evidently located in the inverted region of the Marcus parabola. $Sc_3N@I_h$-C_{80}, such as C_{60}, features small reorganization energies in electron transfer processes. At a larger electron donor-acceptor separation of 46 Å the back ET falls into the normal region of the Marcus parabola.

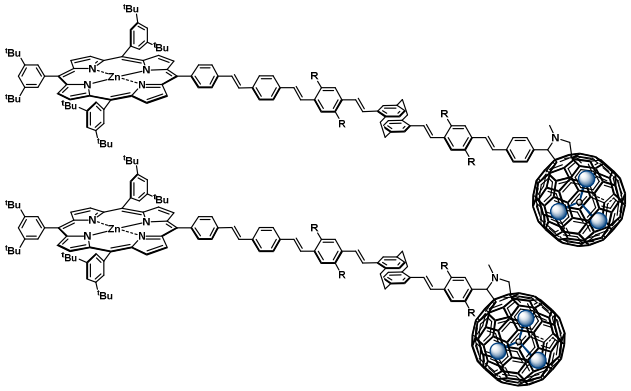

Fig. 14 Structures of porphyrin/endohedral metallofullerene – ZnPor-$Sc_3N@I_h$-C_{80} (I) (top) and ZnPor-$Sc_3N@I_h$-C_{80} (I) (bottom) – based electron donor-acceptor conjugates with R = -C_8H_{17}.[65]

2.2.2. Non-covalently linked electron donor-acceptor hybrids

An alternative to covalently linked electron donor-acceptor conjugates emerges from biomimetic organization principles, such as hydrogen bonding,[35, 66, 67] complementary electrostatics,[68] π-π stacking[69-71] and metal coordination[72]. As in natural photosynthesis, such supramolecular interactions ensure the hierarchical integration of multiple components into well-ordered arrays.[66, 73, 74] These spontaneous organization principles allow designing and devising of novel functional electron donor-acceptor systems and, in turn, predetermined architectures of defined sizes, with high directionality and selectivity.

2.2.2.1 Fullerenes and endohedral metallofullerenes in their ground states

An early example involving EMFs is the complexation of the paramagnetic La@C_{2v}-C_{82} with aza- and thiacrown ethers.[75, 76] Even without photoexcitation La@C_{2v}-C_{82} induces a thermal ET in solution. At complete equilibrium reversible intermolecular spin-site exchange was demonstrated between La@C_{2v}-C_{82} as electron acceptor and various electron donors such as N,N,N',N'-tetramethyl-1,4-phenylendiamin (TMPD), 5,10-dihydro-5,10-dimethylphenazine (DHDMP), and decamethylferrocene ($FeCp^*_2$) –

Scheme 1.[77, 78] Full control over the equilibrium was gained by varying the temperature and/or the solvent. The latter was manifested by a distinct thermo- and solvatochromism. Interestingly, the binding affinities were found to be much stronger than those seen for C_{60}.

Scheme 1: Ground-state ET between La@C_{2v}-C_{82} and TMPD in solution.[77, 78]

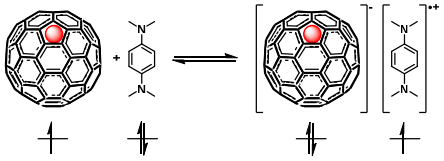

In analogy, the complexation and ET behavior of $La_2@I_h$-C_{80} with two of the aforementioned organic donors (i.e., TMPD and ferrocene) has been studied in solution.[78] In contrast, $La_2@I_h$-C_{80} is diamagnetic. However, it has an exceptionally low LUMO level and the LUMO is localized between the encapsulated La atoms. It is the exceptionally low LUMO level that facilitates a ground-state ET even with diamagnetic $La_2@I_h$-C_{80}. It was demonstrated that $La_2@I_h$-C_{80} forms complexes with TMPD in a 1:1 stoichiometry. Thereby, the equilibrium between TMPD/$La_2@I_h$-C_{80} and $(TMPD)^{\bullet+}$/$(La_2@I_h$-$C_{80})^{\bullet-}$ is readily controlled in solution by the temperature and the solvent.

Scheme 2: Ground-state ET between $[K^+([18]crown-6)]PTM^-$ and Y@C_{2v}-C_{82} giving an anionic Y@C_{2v}-C_{82}-based compound with the complex cation, i.e. $[K^+([18]crown-6)][(Y@C_{2v}$-$C_{82})^-]$ in the solid state.[79]

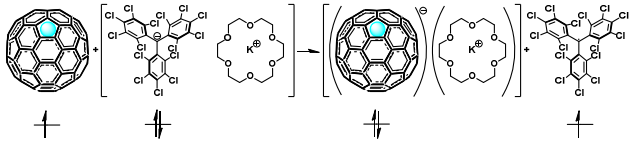

It was demonstrated that the preparation of the $[K^+([18]crown-6)][(Y@C_{2v}$-$C_{82})^{\bullet-}]$ salt is a very promising approach to access novel ionic EMF-based compounds with complex cations.[79] The molar extinction coefficients for both the neutral and anionic forms of Y@C_{2v}-C_{82} were determined in organic solvents of different polarities for the first time; this is of considerable interest for developing the chemistry and physics of monometallofullerenes such as Y@C_{2v}-C_{82}. This new ionic EMF-based compound has revealed outstanding stability both in solution and in the solid state. In contrast to the systems constructed from the paramagnetic lanthanum metallofullerene La@C_{2v}-C_{82} and neutral organic donors reported by Akasaka et. al., this approach is useful for the development of $(M@C_{82})^-$-based salts with different complex cations.

2.2.2.2. Fullerenes and endohedral metallofullerenes in their excited states

The first example, in which C_{60} is linked to an electron-donating ZnPc through a hydrogen-bonding network, generating a pseudorotaxane-like structure – Fig. 15 – was published in 2002.[80] Here, an efficient intracomplex ET process, starting from the ZnPc singlet excited state yielded the $(ZnPc)^{\bullet+}$-$(C_{60})^{\bullet-}$ radical ion pair state, which recombines with a rate constant of 6.7 x 10^5 s^{-1}. In contrast to similar covalently linked ZnPc-C_{60} conjugates,[81] this radical ion pair is about three orders of magnitude longer-lived.

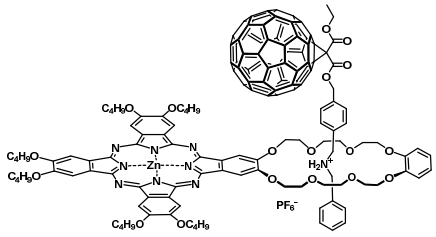

Fig. 15 Structure of a phthalocyanine/fullerene – ZnPc/C_{60} pseudorotaxane – based electron donor-acceptor hybrid.[80]

A study that involves a series of a C_{60} derivative (C_{60}-Py) and two different lanthanum metallofullerene derivatives of La@C_{2v}-C_{82} (La@C_{2v}-C_{82}-Py) and La_2@I_h-C_{80} (La_2@I_h-C_{80}-Py), is especially appealing for the comparison of empty fullerenes and EMFs.[82] All C_{60}s/EMFs feature a pyridyl group as a coordination site for transition-metal ions. It has been shown that a biomimetic organization principle, such as metal-ligand coordination enabled the study of the supramolecular complex formation with ZnPor and photoinduced ET processes of the resulting coordinative electron-donor/electron-acceptor arrays - Fig. 16. However, the binding was dominated by axial coordination, with minor contributions from the orbital overlap of the curved and planar π systems. The binding constants ranged from $\log K_{assoc}$=3.94–4.38. Steady-state as well as time-resolved photophysical techniques revealed that electron transfer governs the excited-state deactivation in all of these systems, namely ZnPor/C_{60}-P, ZnPor/La@C_{2v}-C_{82}-Py, and ZnPor/La_2@I_h-C_{80}-Py. ZnPor served as an excited-state electron donor in this respect. The choice of C_{60}/EMF derivative provides the incentive for controlling the forward ET kinetics (*i.e.* 10^{10} s^{-1}), and the back ET kinetics (*i.e.* 10^{8} s^{-1}), whereas the binding constants are only marginally impacted. Firstly, the lowest reduction potential of La@C_{2v}-C_{82}-Py results in the largest driving force for electron transfer in ZnPor/La@C_{2v}-C_{82}-Py and, therefore, gives the fastest charge separation. Secondly, the SOMO of $[La_2@I_h\text{-}C_{80}]^{\bullet-}$ is localized between the encapsulated La atoms. Any intermolecular overlap with $(ZnPor)^{\bullet+}$ is, therefore, supposed to be small[78, 83, 84] and charge recombination in hindered. Consequently, the slowest charge recombination is found in ZnPor/La_2@I_h-C_{80}-Py.

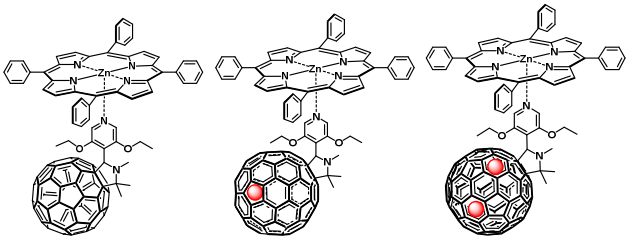

Fig. 16 Structures of porphyrin/fullerene – ZnPor/C_{60}-Py (left) – and porphyrin/endohedral metallofullerene – ZnPor/La@C_{2v}-C_{82}-Py (center) and ZnPor/La_2@I_h-C_{80}-Py (right) – based electron donor-acceptor hybrids.[82]

In another work, the electronic structure of three endohedral fullerene-Zn-tetraphenylporphyrin complexes were studied in the ground and excited state using density functional theory.[85] The binding between the two Sc_3N@I_h-C_{80} or a Y_3N@I_h-C_{80} and ZnPor in these complexes stems from van der Waals interaction. A fragment orbital analysis is carried out to examine the interaction between the two components. It turns out that small charge transfer occurs in the ground state from ZnPor to the endohedral metallofullerenes. Thereby, the orientation of the Sc_3N plane, which distinguishes the two Sc_3N@C_{80} complexes studied here, affects the ground state ET. The charge transfer excited state energies are calculated using a perturbative delta-SCF method. A comparison with earlier calculations shows that the charge transfer excitation energy increases from ZnPor/C_{60} to ZnPor/C_{70} to ZnPor/Sc_3N@I_h-C_{80} to ZnPor/Y_3N@I_h-C_{80}. The orientation of the endohedral unit has no impact on the excitation energy in the electron donor–acceptor arrays. In particular, the CT excitation energies in the co-facial complexes are above 2.0 eV in the gas-phase, which are above the ZnPor lowest singlet excited state. We find that going from Sc_3N@I_h-C_{80} to Y_3N@I_h-C_{80} at the acceptor part may result in larger CT excitation energy and lower exciton binding energy. The results are obtained in the gas-phase, thus, in a solution or in the aggregated form, the excitation energies may change due to polarization effects.

More recent work features the combination of different supramolecular binding motifs, so called cooperative binding.[68, 86-89] For instance, a guanidinium bis-ZnPor tweezers is able to form a hybrid with a C_{60}-carboxylate – Fig. 17 – via hydrogen bonding as well as π-π stacking, featuring exceptionally high binding constants (10^6 M^{-1}).[86] Upon photoexcitation the hybrid undergoes ET, generating nanosecond-lived radical ion pair states, involving the singly reduced C_{60} and the singly oxidized tweezers.

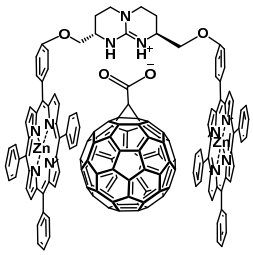

Fig. 17 Structure of a porphyrin/fullerene – guanidinium bis-ZnPor/C_{60}-carboxylate – based electron donor-acceptor hybrid.[86]

2.3. EnT and reductive ET – see Fig. 1

2.3.1. Covalently linked electron donor-acceptor arrays

Myriad of examples to device antenna systems with suitable energetic as well as spatial arrangements are known. Hexaphenylbenzene, for example, were utilized as a core, to which up to six chromophores are linked.[90-94] In this context, different combinations of chromophores were organized around the central hexaphenylbenzene core. In a leading example, five bis-(phenylethynyl)anthracene (BPEA) antennas are combined with a porphyrin-fullerene conjugate.[91] Alternatively, the combinations of two BPEAs, two BODIPYs and two ZnPors[93], or four coumarins and two ZnPor[90] – Fig. 18 – have been explored. Light is absorbed in any of the mentioned systems in the visible region of the spectrum by the BPEA, BODIPY and coumarin antennas. Subsequently, the excitation energy is transferred very efficiently with quantum yields of up to 1.0 to the ZnPors via singlet-singlet EnT. Both, a direct as well as a stepwise funnel-like pathway enables EnTs within the ps time scale via the Förster mechanism, as in natural photosynthesis.

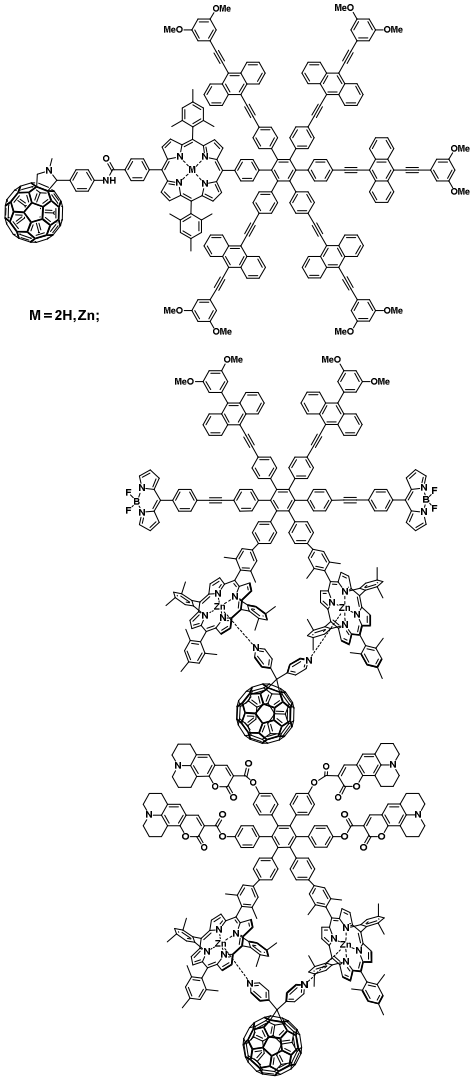

Fig. 18 Structures of hexaphenylbenzene based antenna-reaction center conjugates.[90, 91, 93]

In a recent example, a photosynthetic antenna-reaction center model combines the benefits of a ZnPor and a ZnPc with those of triphenylamine (TPA) – Fig. 19 – resulting in a stepwise EnT from the singlet excited state of TPA to ZnPor and to ZnPc with rate constants of ~ 10^{11} s^{-1}.[95]

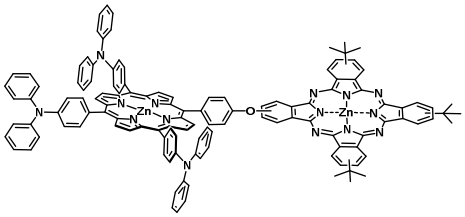

Fig. 19 Structure of the tris(triphenylamine)/zinc porphyrin/zinc phthalocyanine – TPA-ZnPor-ZnPc – based antenna-reaction center conjugate.[95]

2.4. Cascades of EnT and ET – see Fig. 1

2.4.1. Covalently linked electron donor-acceptor arrays

As an alternative to molecular wires, which force the electron transfer through a single, concerted long distance step, charges can also be transported over longer distances (> 20 Å) by a relay/cascade of several short distance electron transfer steps along well designed redox gradients. Several redox active building blocks, such as carotenoids (C), TTF, Fc, ZnPor, H_2Por, etc. were combined with fullerenes, in order to generate long lived radical ion pairs.

Remarkable examples of this relay approach are Fc-H_2Por-C_{60}, Fc-ZnPor-C_{60}, Fc-ZnPor-H_2Por-C_{60}, and Fc-ZnPor-ZnPor-C_{60} - Fig. 20[27, 28] – where the final electron donors (i.e., Fc) and the primary electron acceptors (i.e., C_{60}) are separated by distances of up to 50 Å. As an example, Fc-ZnPor-H_2Por-C_{60}[27] mimics all the primary events seen in photosynthesis upon photoexcitation, that is, LH, EnT, ET, and electron shift. To be more precise, ZnPor performs as an antenna that transfers its singlet excited state energy to the energetically lower lying H_2Por. Subsequent to this EnT, a sequential ET relay takes place, evolving from the generated singlet excited state of H_2Por to give, initially, the adjacent $(H_2Por)^{\bullet+}/(C_{60})^{\bullet-}$, then the intermediate $(ZnPor)^{\bullet+}/(C_{60}^{\bullet-})$, and, finally, the distant $(Fc)^{\bullet+}/(C_{60})^{\bullet-}$ radical ion pair states. Here, ZnPor-H_2Por, acts as a bridge, into which the charges are intermediately stored. In the same way, H_2Por, ZnPor, and ZnPor-ZnPor are the bridges in Fc-H_2Por-C_{60}, Fc-ZnPor-C_{60}, and Fc-ZnPor-ZnPor-C_{60}, respectively. The substitution of H_2Por by ZnPor[28] leads to further advances in terms of efficiency and lifetime, since this raises the excited state energy of the chromophore from approximately 1.89 to 2.04 eV. Additionally, the oxidation potential of the electron donor is lowered by nearly 300 mV. Consequently, in Fc-ZnPor-ZnPor-C_{60} larger -ΔG° values for the initial electron transfer and, in turn, higher efficiencies and 34% slower charge recombination, i.e. k_{CR} = 0.62 s^{-1}, are yielded, compared to Fc-ZnPor-H_2Por-C_{60}. In the context of molecular mimic of the photosynthetic reaction center the lifetimes of the distant $(Fc)^{\bullet+}/(C_{60})^{\bullet-}$ radical ion pair states as the product of a cascade of energy and sequential ET reactions in Fc-ZnPor-H_2Por-C_{60} and in Fc-ZnPor-ZnPor-C_{60} reach a time domain that has never been accomplished so far. The lifetimes are also comparable to those of the bacterio-chlorophyll dimer radical cation $((Bchl)_2^{\bullet+})$/secondary quinone radical anion $(QB^{\bullet-})$ ion pair in the bacterial photosynthetic reaction center. When comparing the charge recombination rates in Fc-ZnPor-H_2Por-C_{60} (2.6 s^{-1}) and Fc-ZnPor-ZnPor-C_{60} (0.62 s^{-1}) with those seen for the single step electron transfers in Fc-C_{60} (> 10^6 s^{-1})[39], H_2Por-C_{60} (10^7 s^{-1}), and ZnPor-C_{60} (7.7 x 10^5 s^{-1})[46] differences of six orders of magnitude, that is, seconds versus microseconds and more become evident. Such outstanding lifetimes can be rationalized by very small electronic coupling elements of (5.6 ± 0.5) × 10^{-5} cm^{-1} in Fc-ZnPor-ZnPor-C_{60} relative to, for example, a value of 7.9 ± 1.7 cm^{-1} seen for ZnPor-C_{60}, where the separations are ~12 Å. This finding correlates with negligible orbital overlap and a rather high attenuation factor of 0.60 $Å^{-1}$,[96] gathered from a linear but steep relationship between radical ion pair lifetimes, on one hand, and electron-donor-acceptor separations, on the other hand.

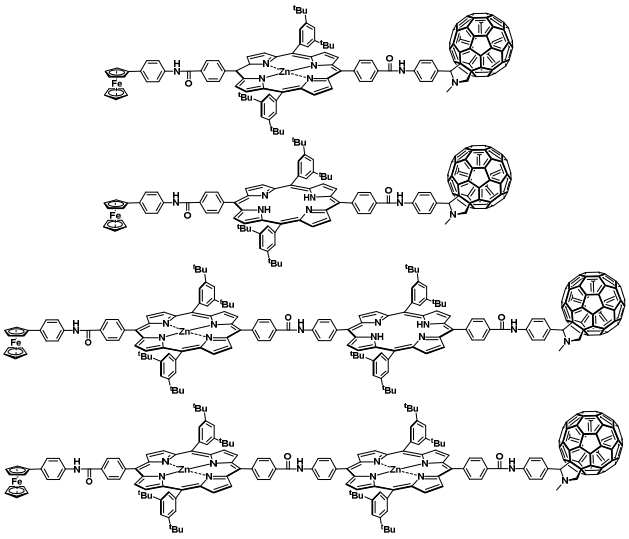

Fig. 20 Structures of ferrocene/porphyrin/fullerene – Fc-ZnPor-C_{60} (top), Fc-H_2Por-C_{60} (middle top), Fc-ZnPor-H_2Por-C_{60} (middle bottom), and Fc-ZnPor-ZnPor-C_{60} (bottom) – based electron donor-acceptor arrays.[27, 28]

Fig. 21 surveys a few examples of BF_2-chelated azadipyrromethene (azaBODIPY) building blocks in combination with fullerenes and Fc/phenothiazine (PTZ) electron donors as a platform to study the influence of electron donor-acceptor distances, orientations, and excitation wavelengths on the efficiency and mechanism of ET reactions.[97-99] In $(Fc)_2$-azaBODIPY-C_{60}[98] and $(PTZ)_2$-azaBODIPY-C_{60}[99] only a single step ET is found to generate radical ion pairs in the form of $(Fc)_2^{\bullet+}$-azaBODIPY-$(C_{60})^{\bullet-}$ and $(PTZ)_2$-$(azaBODIPY)^{\bullet+}$-$(C_{60})^{\bullet-}$, respectively, which recombine with rates in the order of 10^{10} s^{-1}. In stark contrast, in BODIPY-azaBODIPY-C_{60} a multistep ET affords radical ion pairs $(BODIPY)^{\bullet+}$-azaBODIPY-$(C_{60})^{\bullet-}$ with charge recombination rates of 5-6 x 10^8 s^{-1}.[97]

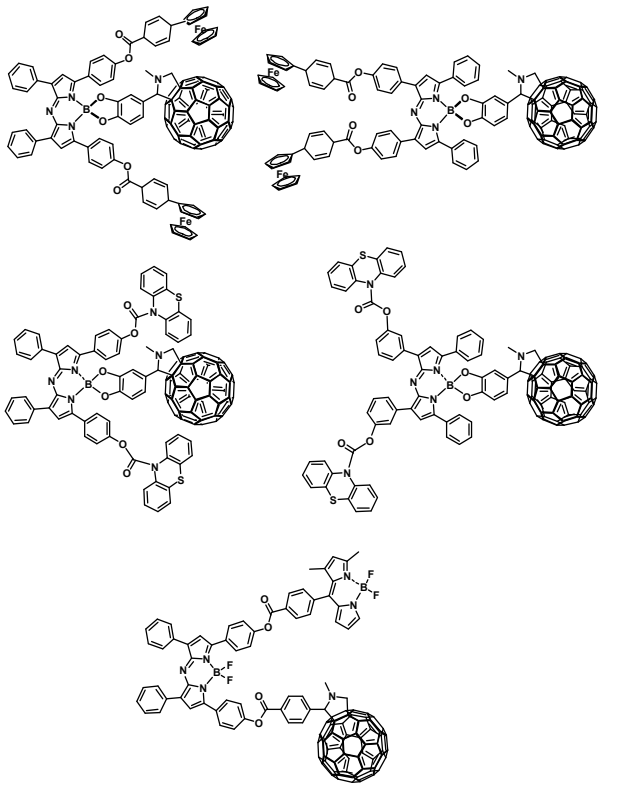

Fig. 21 Structures of azaBODIPY/fullerene – $(Fc)_2$-azaBODIPY-C_{60} (top), $(PTZ)_2$-azaBODIPY-C_{60} (middle), and BODIPY-azaBODIPY-C_{60} (bottom) – based electron donor-acceptor arrays.[97-99]

2.4.2. Mechanically interlocked electron donor-acceptor hybrids

Another important aspect for the successful design of artificial photosynthetic systems is the appropriate spatial arrangement of the different chromophores, which can be accomplished through covalent linkage[30, 100-103] or via supramolecular interactions[30, 102-106], as described above. An interesting alternative to spatially arrange the chromophores is provided by mechanically-interlocked systems, such as catenanes and rotaxanes, decorated with C_{60} as electron accpetor and various electron donors - Fig. 22.[107-109] For example, a catenane[110] decorated with ZnPor and C_{60} undergoes a sequence of EnT and ET processes along a redox gradient, ultimately yielding a radical ion pair state possessing $(ZnPor)^{\bullet+}$ and $(C_{60})^{\bullet-}$ with a charge recombination rate of 9.1 x 10^5 s^{-1}, roughly two times slower than the same charge separated state in the rotaxane analog.[111] This significant difference in lifetime reflects the distinct topology of the two interlocked systems. The catenane is conformationally rigid, while the rotaxane counterpart is not. Therefore, the former keeps the ZnPor and C_{60} moieties at longer and fixed distance, while the latter brings them closer to each other, a process that is driven by secondary interactions between the chromophores and allowed by the unclosed ring of the rotaxane.[110-118] However, when 1,4-diazabicyclo[2.2.2]-octane (DABCO) is added to the rotaxane bearing two ZnPor stoppers, the central metal serves as recognition site for complexation and a bridge between the two ZnPors of the rotaxane is formed, generating a catenane-like structure, resulting in a radical ion pair state lifetime comparable to those observed in the catenane.[110, 111] When replacing ZnPor in the catenated system by

MgPor or H_2Por, analog processes take place, however ET is not enhanced, in spite of MgPor's low oxidation potential (0.07 V compared to 0.28 V in ZnP in *o*-DCB vs. Fc/Fc^+) and radical ion pairs are shorter lived.[119] Another decisive fact for the ET to take place in the investigated catenanes and rotaxanes is the presence of the central $[Cu(phen)_2]^+$ moiety. When the Cu(I) ion is removed from the $(ZnPor)_2/[Cu(phen)_2]^+$-C_{60} rotaxane, major structural changes occur and photoinduced ET no longer takes place. From those results it is deduced that the central $[Cu(phen)_2]^+$ moiety is of critical importance for the long-range ET in the investigated interlocked systems and serves as a mediator in the ET chain.[111] A significantly slower charge recombination rate for $(ZnPor)^{\bullet+}/[Cu(phen)_2]^+/(C_{60})_2^{\bullet-}$ of 3.1 x 10^4 s^{-1} could be achieved in C_{60} stoppered porphyrinorotaxanes[113] – Fig. 22 top left, since here the close approach of ZnPor and C_{60} moieties is excluded. Further variations in the rotaxanes, namely exchanging the electron donating moieties leads to different results. When the ZnPor stoppers are replaced by Fc, which is easier to oxidize than the porphyrins and, thus, lowered the energy level of the CS state, long range ET is inhibited and only the ns-lived $(Fc)_2/[Cu(phen)_2]^{2+}/(C_{60})_2^{\bullet-}$ is observed, without any appreciable evidence for a subsequent charge shift to the Fcs.[115] However, when replacing just one of the ZnPor stoppers by Fc, a charge shift from ZnP to the ferrocene takes place to yield the thermodynamic more stable Fc-centered charge separated state $ZnPor/(Fc)^{\bullet+}/[Cu(phen)_2]^+/(C_{60})_2^{\bullet-}$, with a charge recombination rate of 1.6 x 10^4 s^{-1}.[120] Furthermore, also ZnPc was introduced as electron donor to the $[Cu(phen)_2]^+$-based rotaxanes, on one hand, in combination with ZnPor, on the other hand, together with Fc. Again multistep EnT and ET was observed, generating long lived radical ion pair states, including singly oxidized $[Cu(phen)_2]^+$, ZnPor, ZnPc or Fc and singly reduced C_{60}, with charge recombination rates of 1-2 x 10^5 s^{-1}.[120]

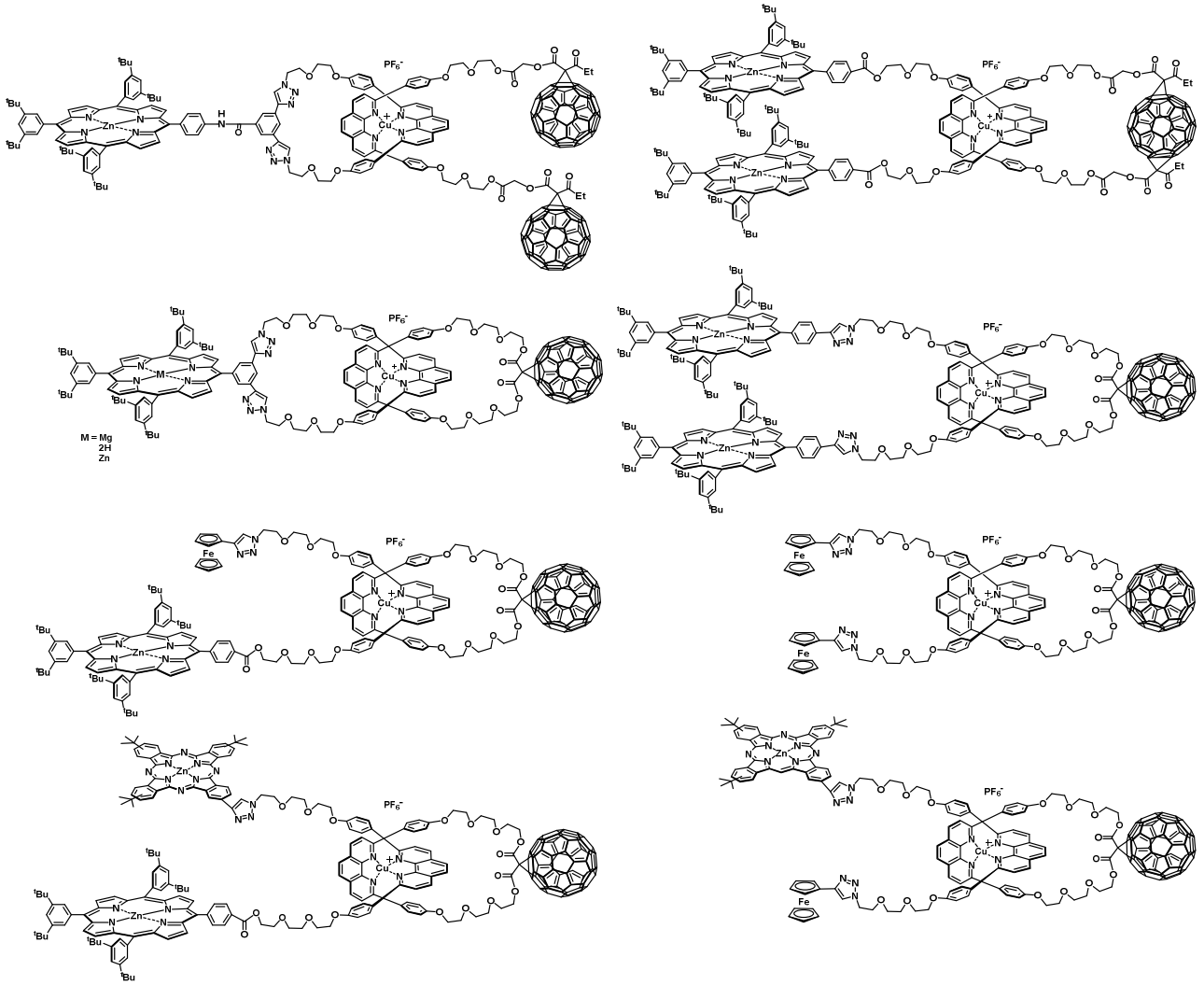

Fig. 22 Structures of porphyrin/$[Cu(phen)_2]^+$/fullerene – ZnPor/$[Cu(phen)_2]^+/(C_{60})_2$ (top left), $(ZnPor)_2/[Cu(phen)_2]^+/C_{60}$ (2x) (top right and middle top right), ZnPor/$[Cu(phen)_2]^+/C_{60}$ (middle top left) – porphyrin/ferrocene/$[Cu(phen)_2]^+$/fullerene – ZnPor/Fc/$[Cu(phen)_2]^+/C_{60}$ (middle bottom left – ferrocene/$[Cu(phen)_2]^+$/fullerene - $(Fc)_2/[Cu(phen)_2]^+/C_{60}$ (middle bottom right)) – phthalocyanine/porphyrin/$[Cu(phen)_2]^+$/fullerene – ZnPc/ZnPor/$[Cu(phen)_2]^+C_{60}$ (bottom left) – phthalocyanine/ferrocene/$[Cu(phen)_2]^+$/fullerene – ZnPc/Fc/$[Cu(phen)_2]^+/C_{60}$ (bottom right) –based electron donor-acceptor catenanes and rotaxanes.[110, 111, 113-115, 119, 120]

Journal Name

ARTICLE

2.5. Switchable ET / reductive or oxidative ET – see Fig. 1

Two studies among the early work of photoinduced ET with endohedral metallofullerenes underpin their highly amphotheric nature in electron transfer processes.[121, 122] Stable, covalently linked conjugates of ZnPor, on one hand, and $M_2@I_h$-C_{80} (M = Ce or La) or $Sc_3N@I_h$-C_{80}, on the other hand, have been prepared – Fig. 23. Steady-state absorption spectroscopy and electrochemistry documents appreciable interactions in the ground state that are rationalized by a close-contact geometry as well as unusual strong π-π and electrostatic interactions. Density functional calculations reveal that in the lowest energy conformations assume van der Waals distances. Photophysical assays corroborate a quite remarkable effect of the endohedral cluster on the charge transfer chemistry. Whereas photoexcitation of ZnPor-$Sc_3N@I_h$-C_{80} affords the same $(ZnPor)^{\bullet+}$-$(Sc_3N@I_h\text{-}C_{80})^{\bullet-}$ radical ion pair regardless of the solvent polarity, the outcome of photoinduced charge transfer for ZnPor-$M_2@I_h$-C_{80} varies with solvent polarity. Notably, ET evolving from the ZnPor singlet excited state (2.0 eV) is thermodynamically feasible in all the tested solvents ranging from toluene to DMF since the $(ZnPor)^{\bullet-}$-$(M_2@I_h\text{-}C_{80})^{\bullet+}$ radical ion pair energies have energy levels ranging from 0.72 eV (toluene) to 0.45 eV (DMF) for $(ZnPor)^{\bullet-}$-$(La_2@I_h\text{-}C_{80})^{\bullet+}$ and from 0.78 eV (toluene) to 0.49 eV (DMF) for $(ZnPor)^{\bullet-}$-$(Ce_2@I_h\text{-}C_{80})^{\bullet+}$. On the contrary, the $(ZnPor)^{\bullet+}$-$(M_2@I_h\text{-}C_{80})^{\bullet-}$ radical ion pairs are associated with energies with the highest value in toluene (2.3 eV) exceeding the one of the singlet excited ZnPor. When more polar solvents such as benzonitrile or DMF are used the $(ZnPor)^{\bullet+}$-$(M_2@I_h\text{-}C_{80})^{\bullet-}$ radical ion pair state becomes thermodynamically accessible by singlet excited ZnPor. In other words, reduction of the highly localized $[M_2]^{6+}$ cluster is sufficiently exothermic in all solvents. The electronic coupling is weak between the $[M_2]^{6+}$ cluster and the electron-donating ZnPor. The oxidation of $(C_{80})^{6-}$ and the simultaneous reduction of ZnPor, on the other hand, necessitate solvent stabilization. In that case, the strongly exothermic $(ZnPor)^{\bullet-}$-$(M_2@I_h\text{-}C_{80})^{\bullet+}$ radical ion pair state formation is compensated by a nonadiabatic charge transfer and the ZnPor/$(C_{80})^{6-}$ electronic matrix element exceeds that for ZnPor/$[M_2]^{6+}$. Notably the product of charge recombination is also different. On one hand, $(ZnPor)^{\bullet+}$-$(M_2@I_h\text{-}C_{80})^{\bullet-}$ recombines to the singlet ground state, on the other hand, $(ZnP)^{\bullet-}$-$(M_2@I_h\text{-}C_{80})^{\bullet+}$ gives the triplet excited state of the dimetallofullerenes. Rate constants for charge separation were found to be ultrafast on the timescale of 10^{12} s^{-1} for ZnPor-$Ce_2@I_h$-C_{80} and even faster for ZnPor-$La_2@I_h$-C_{80} (>10^{12} s^{-1}). A thorough kinetic analysis lead to charge recombination rate constants of 1.8 x 10^{10} (benzonitrile), 8.6 x 10^9 s^{-1} (DMF) for ZnPor-$Ce_2@I_h$-C_{80} as well as 4.3 x 10^9 (toluene), 5.8 x 10^9 (THF), 1.8 x 10^9 (benzonitrile), and 1.6 x 10^{10} s^{-1} (DMF) for ZnPor-$La_2@I_h$-C_{80}.

The solvent dependent electron transfer with the dimetallofullerenes $M_2@I_h$-C_{80} is a promising way to tune the outcome of photoinduced electron transfer events. So, EMFs can not only be considered as n-type but also as unprecedented p-type fullerene material for a solar energy conversion system. Likewise, this paves the way en route towards purely oxidative electron transfer with EMFs as electron donors as new possibilities for fundamental processes of water oxidation triggered by light.[123]

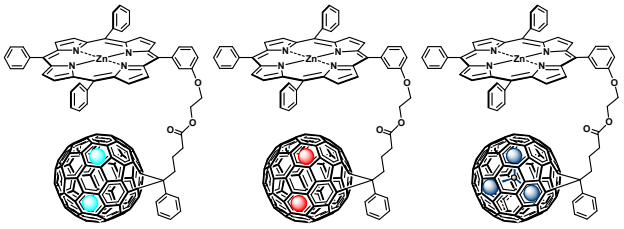

Fig. 23 Structures of porphyrin/endohedral metallofullerene – ZnPor-$Ce_2@I_h$-C_{80} (left), ZnPor-$La_2@I_h$-C_{80} (center), and $Sc_3N@I_h$-C_{80}-ZnPor (right) – based electron donor-acceptor conjugates.[121, 122]

2.6. Oxidative ET – see Fig. 1

2.6.1. Covalently linked electron donor-acceptor conjugates

2.6.1.1. Fullerenes and endohedral metallofullerenes in their excited states

Oxidation of fullerenes usually requires harsh conditions. Thus, oxidation occurs only by treating them with, for example, strong oxidizing agents[124-126] or upon photo- or electron-induced ionization in the presence of electron transferring photosensitizers.[127-129] In the first example of intermolecular ET oxidation of empty fullerenes the presence of *p*-benzoquinone and radical ion pair stabilizing scandium triflate $Sc(OTf)_3$ facilitate an oxidative electron transfer.[130]

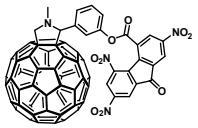

Fig. 24 Structures of a fullerene/trinitrofluorenone – C_{60}-TNF – based electron donor-acceptor conjugate.[131]

For a long time just a single case of intramolecular oxidation of fullerenes has been reported – Fig. 24.[132] In a fullerene-trinitrofluorenone conjugate, photoexcitation leads to the formation of oxidized C_{60}, and reduced TNF. However, this unprecedented ET event only occurs in the presence of radical ion pair stabilizing $Sc(OTf)_3$, whereas the triplet excited state of the fullerene was observed in the absence of the latter.[131]

$La_2@I_h$-C_{80}-TCAQ (see Fig. 25), where $La_2@I_h$-C_{80} is covalently linked to the strong electron acceptor 11,11,12,12-tetracyano-9,10-anthra-p-quinodimethane (TCAQ), was one of the early studies that demonstrated oxidative electron transfer to be operative from the electron donating $La_2@I_h$-C_{80} to the electron accepting TCAQ to give the $(La_2@I_h\text{-}C_{80})^{\bullet+}$-$(TCAQ)^{\bullet-}$ radical ion pair state in nonpolar as well as polar media.[133] In the ground state weak electronic coupling dictates the interactions between $La_2@I_h$-C_{80} and TCAQ. However, $La_2@I_h$-C_{80} in its singlet excited state (1.4 eV) powers an electron transfer that yields a spatially separated radical ion pair state (1.15 eV). The one-electron reduced TCAQ and the one-electron oxidized $La_2@I_h$-C_{80} decay with a rate constant of up to 4.4 x 10^9 s^{-1} to recombine to the triplet excited state (1.0 ± 0.1 eV) of $La_2@I_h$-C_{80}. In this electron donor-acceptor conjugate it is both the strong electron acceptor character of TCAQ and the strong electron donor character of $La_2@I_h$-C_{80} that are decisive to afford the radical ion pair state independent on solvent polarity.

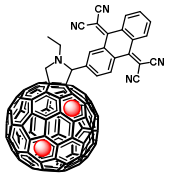

Fig. 25 Structure of $La_2@I_h$-C_{80}-TCAQ.[133]

Two studies report the synthesis and full-fledged photophysical analysis of two covalently linked $Lu_3N@I_h$-C_{80}-perylenebisimide (PDI) conjugates (Fig. 26). ET evolves from the electron donating $Lu_3N@I_h$-C_{80} to the electron accepting PDI singlet excited state (2.32 eV) to yield the $(Lu_3N@I_h\text{-}C_{80})^{\bullet+}$-$(PDI)^{\bullet-}$ radical ion pairs (1.43 eV).[134, 135] The latter is metastable and decays in the flexible $Lu_3N@I_h$-C_{80}-PDI conjugate with rate constants of 8.3 x 10^9 s^{-1} in toluene, 1.0 x 10^{10} s^{-1} in chlorobenzene and 2.2 x 10^{10} s^{-1} in benzonitrile. Product of charge recombination is the PDI triplet excited state. The flexible linkage, however, turned out to be unfavourable for long-lived charge separation.

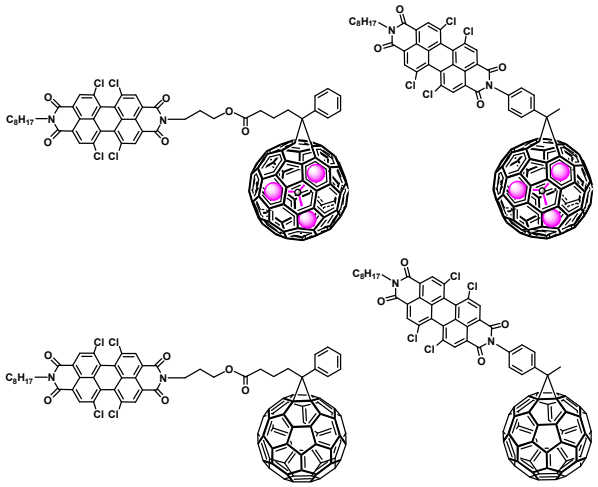

Fig. 26 Structures of endohedral metallofullerene/PDI – $Lu_3N@I_h$-C_{80}-PDI (top) – and fullerene/PDI – C_{60}-PDI (bottom) – based electron donor-acceptor conjugates.[135]

In the rigidly linked or linear electron donor-acceptor conjugate of $Lu_3N@I_h$-C_{80} and PDI the presence of the Lu_3N cluster exerts an appreciable electron nuclear hyperfine interaction on the charge transfer dynamics. Although photoexcitation of PDI also leads to an ultrafast PDI singlet excited state decay that results in ET, i.e., to the $(Lu_3N@I_h\text{-}C_{80})^{\bullet+}$-$(PDI)^{\bullet-}$ radical ion pair state, the consecutive processes differ dramatically. The initially formed singlet radical ion pair state, $^1[(Lu_3N@I_h\text{-}C_{80})^{\bullet+}\text{-}(PDI)^{\bullet-}]$, undergoes radical ion pair intersystem crossing facilitated by electron nuclear hyperfine coupling induced by the presence of the Lu_3N cluster. The product of this process is the triplet radical ion pair state, $^3[(Lu_3N@I_h\text{-}C_{80})^{\bullet+}\text{-}(PDI)^{\bullet-}]$. Back ET from the triplet radical ion pairs to reinstate the singlet ground state is spin-forbidden and, therefore, potentially slower than that seen from singlet radical ion pairs. In this study it was possible to obtain, on one hand, rate constants for the singlet radical ion pair state as short as 3.6 x 10^{10} s^{-1} (DMF) and, on the other hand, the rate constant for the triplet radical ion pair state as long as 9.8 x 10^6 s^{-1} (THF). Most notably, the radical ion pair state lifetime was, thereby, increased by over three orders of magnitude.

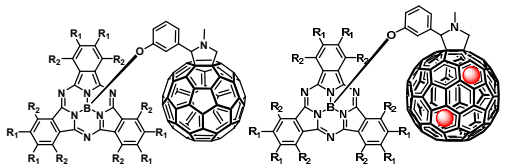

Fig. 27 Structures of fullerene/subphthalocyanine – C_{60}-SubPc (left) – and endohedral metallofullerene/subphthalocyanine – $La_2@I_h$-C_{80}-SubPc (right) – based electron donor-acceptor conjugates.[136, 137]

In another publication electron accepting SubPcs have been combined with $La_2@I_h$-C_{80} to prepare a series of novel $La_2@I_h$-C_{80}-SubPc electron donor–acceptor conjugates to mimic the photosynthetic apparatus – Fig. 27.[136] In the excited state an intramolecular ET evolves from $La_2@I_h$-C_{80} to photoexcited SubPc to give energetically low-lying radical ion pair states, i.e., $(La_2@I_h\text{-}C_{80})^{\bullet+}$-$(F_{12}SubPc)^{\bullet-}$ (1.32 eV) or $(La_2@I_h\text{-}C_{80})^{\bullet+}$-$((SO_2C_5H_{11})_6SubPc)^{\bullet-}$ (1.36 eV) ,consisting of the one-electron-oxidized $La_2@I_h$-C_{80} and of the one-electron-reduced SubPc. The SubPc singlet excited states decay with 7.1 x 10^{11} s^{-1} and 3.3 x 10^{11} s^{-1} to give the aforementioned radical ion pair states. The singlet ground state is reinstated with rate constants from 3.6 x 10^{10} to 2.9 x 10^{10} s^{-1}. One should keep in mind that the short separation between the electron donors and acceptors still allows for optimization of the radical ion pair state lifetimes *via* the tailored design of linkers between SubPc and $La_2@I_h$-C_{80}. In comparison, reference conjugates of C_{60} and SubPcs under identical experimental conditions feature only a singlet-singlet energy transfer from SubPc to C_{60} followed by a C_{60} centered intersystem crossing and a triplet-triplet energy transfer back to the SubPc. Thus, replacing C_{60} by $La_2@I_h$-C_{80} provides a promising way to tune the outcome of photoinduced processes, *i.e.* energy-transfer versus electron-transfer. The first singlet excited states of the C_{60}-SubPcs , i.e., F_{12}SubPc (2.16 eV), $(SO_2C_5H_{11})_6$SubPc (2.12 eV), or C_{60} (1.8 eV), are insufficient in terms of thermodynamic driving force to power an electron transfer. Only higher lying singlet excited states (S_2 states of F_{12}SubPc (3.4 eV) and $(SO_2C_5H_{11})_6$SubPc) (3.3 eV)) provide enough thermodynamic driving force to power ultrafast ET events from C_{60} to the electron accepting subphthalocyanines to yield the

$(C_{60})^{\bullet+}$-$(F_{12}SubPc)^{\bullet-}$ (2.17 eV) or $(C_{60})^{\bullet+}$-$((SO_2C_5H_{11})_6SubPc)^{\bullet-}$ (1.95 eV). This finding is of particular importance, since it is the first case of an intramolecular oxidation of C_{60} as part of an electron donor acceptor conjugate. Rate constants for forward ET were determined ranging from 1.7 x 10^{12} s^{-1} to 2.4 x 10^{11} s^{-1} and for back ET between 6.3 x 10^{10} s^{-1} and 2.6 x 10^{10} s^{-1}.[137]

2.6.2. Non-covalently linked electron donor-acceptor hybrids

2.6.2.1. Fullerenes and endohedral metallofullerenes in their excited states

Scheme 3: Small reorganization energies of photoinduced electron transfer between spherical fullerenes.[138]

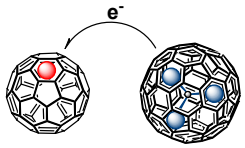

Another study probed the exceptional low reorganization energies of photoinduced ET between different endohedral metallofullerenes or C_{60} – Scheme 3.[138] It was demonstrated that intermolecular ET occurs from either $Sc_3N@I_h$-C_{80} or C_{60} to the triplet excited state of the lithium-ion encapsulated $Li^+@C_{60}$ (1.67 eV) upon nanosecond laser excitation with 355 nm in benzonitrile solutions. In the latter case, that is, ET from $Sc_3N@I_h$-C_{80} to the triplet excited state of $Li^+@C_{60}$ resulted in the formation of the one electron oxidized $(Sc_3N@I_h\text{-}C_{80})^{\bullet+}$ and the one electron reduced $(Li^+@C_{60})^{\bullet-}$ with a bimolecular rate constant of k_{ET} = 1.9 x 10^9 M^{-1} s^{-1} close to the diffusion limited value in benzonitrile (5.6 x 10^9 M^{-1} s^{-1}). The rate of back ET from $(Li^+@C_{60})^{\bullet-}$ to $(Sc_3N@I_h\text{-}C_{80})^{\bullet+}$ was also determined to be k_{ET} = 1.9 x 10^9 M^{-1} s^{-1}. The driving forces for forward ET and back ET were calculated from electrochemical data and were $-\Delta G_{ET}$ = 0.58 eV and $-\Delta G_{ET}$ = 0.95 eV. C_{60} is far more difficult to oxidize than $Sc_3N@I_h$-C_{80} resulting in an just slightly exergonic driving force for oxidative charge transfer of $-\Delta G_{ET}$ = 0.09 eV. Although it was also possible to observe oxidative ET between C_{60} and $Li^+@C_{60}$ after photoexcitation to give $(C_{60})^{\bullet+}$ and $(Li^+@C_{60})^{\bullet-}$ with 50 % quantum yield and a bimolecular decay rate constant of k_{ET} = 2.6 x 10^9 M^{-1} s^{-1}. The back ET from $(Li^+@C_{60})^{\bullet-}$ to $(C_{60})^{\bullet+}$ produces the triplet excited states of $^{3*}(Li^+@C_{60})$ and $^{3*}C_{60}$ rather than the ground state of $Li^+@C_{60}$ or C_{60}. The driving force dependence of $logk_{ET}$ and $logk_{BET}$ was well fit by using the Marcus theory of outer-sphere electron transfer. The internal reorganization energy λ_i was estimated by DFT calculations and the solvent reorganization energy λ_s was calculated by the Marcus equation. When benzonitrile was replaced by o-dichlorobenzene, the overall reorganization energy decreased because of the smaller solvation stabilization of the highly spherical fullerenes upon electron transfer in a less polar solvent. The internal reorganization energies λ_i for electron transfer were determined to be smaller than 0.12 eV and smaller than 0.16 eV for the $Sc_3N@I_h$-$C_{80}/Li^+@C_{60}$ and $C_{60}/Li^+@C_{60}$ electron donor-acceptor couples, respectively.

The supramolecular host-guest interactions of a calixarene scaffold bearing H_2Por or ZnPor as hosts with C_{60}, $Sc_3N@I_h$-C_{80}, and $Lu_3N@I_h$-C_{80} as guests were probed with different spectroscopical and electrochemical techniques.[71] Job's plot analysis revealed a 1:1 stoichiometry. The exponential relationship of fullerene/EMF concentration on the porphyrin fluorescence was used to quantify the association between the bisporphyrins and the fullerenes. Interestingly, the binding constants of $Sc_3N@I_h$-C_{80}, and $Lu_3N@I_h$-C_{80} ($logK_{ass}$≈5) with the two different bisporphyrins were two order of magnitude higher when compared to C_{60} ($logK_{ass}$≈3). The endohedral fullerenes show the existence of an oxidative ET upon photoexcitation to yield the $(Sc_3N@I_h\text{-}C_{80})^{\bullet+}$ or $(Lu_3N@I_h\text{-}C_{80})^{\bullet+}$ and the corresponding radical anions of the bisporphyrins. In contrast, the directionality of ET within the C_{60} containing supramolecular hybrids is reversed, namely yielding the C_{60} radical anion and the bisporphyrin cations. The fastest charge separation (2.0 x 10^{10} s^{-1}) and recombination (3.5 x 10^9 s^{-1}) was observed with $Lu_3N@I_h$-C_{80} and free-base porphyrin, whereas the slowest forward ET (1.0 x 10^{10} s^{-1}) and back ET (6.9 x 10^8 s^{-1}) was found for C_{60} and H_2Por.

2.7 CAT - see Fig. 1

In terms of photocatalysis, only a few examples using fullerenes are known. For photocatalysis to take place, the radical ion pair needs to be long lived. This is, for instance, the case in the ZnPor-C_{60} and ZnPor-H_2Por-C_{60} electron donor-acceptor arrays[139]. The photolytically generated $(C_{60})^{\bullet-}$ and $(ZnPor)^{\bullet+}$ react with NADH analogues (1-benzyl-1,4-dihydronicotinamide and 10-methyl-9,10-dihydroacridine) via one electron reduction and with hexyl viologen (HV^{2+}) via one electron oxidation, respectively – Scheme 4. In benzonitrile the electron donor-acceptor conjugates act as efficient photocatalysts for the uphill oxidation of NADH analogues by HV^{2+}.

Scheme 4: Scheme for the ZnP-C_{60} catalyzed uphill photooxidation of BNAH by HV^{2+}.

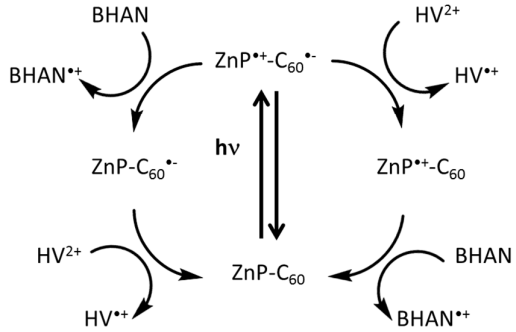

Recent research efforts were directed towards photoelectrochemical splitting of water into hydrogen and oxygen using an organic photodevice responsive to a broad visible absorption range up to 750 nm. Organic p/n bilayer photocathodes were prepared with H_2Pc and C_{60}. Thereby, Pt was loaded onto C_{60}. Upon irradiation the doubly reduced $(C_{60})^{2-}$ is formed, which itself possesses reducing power for H_2 evolution. With support of spectroelectrochemical experiments the authors support that $(C_{60})^{2-}$ is the active species participating in the H_2 evolution.[140, 141]

Further, an organic p/n bilayer system of ZnPc and C_{60} was used for the oxidative decomposition of hydrazine (N_2H_4) into N_2, simultaneously yielding H_2 from H^+ with high faradaic efficiencies. Here, the

photocatalytic oxidation of N_2H_4 to N_2 occurs at the ZnPc/water interface. Reduction of H^+ to H_2 takes place at a Pt wire, to which the reducing power photogenerated at C_{60} is transferred. Pt-loaded C_{60} in the ZnPc/C_{60} bilayer induces the evolution of H_2 under acidic conditions. The Pt-wire clearly functions a co-catalyst for H_2 evolution in this case.[142]

3. Conclusion

This review article highlights artificial model systems, featuring empty fullerenes and/or EMFs, which mimic the key steps of natural photosynthesis, namely LH, EnT, ET, and CAT. In the context of the Marcus theory and different mechanisms for EnT processes, certain aspects have to be considered in the rational design of such photosynthetic mimics. On one hand, chromophores that efficiently harvest solar light have to be chosen. On the other hand, the energy donors and acceptors need to exhibit matching energetics and overlapping electron density, respectively, in order to efficiently transfer excited state energy. Furthermore, for efficient ET, suitable redox properties of the electron donors and acceptors are required. In case of multistep ET, a redox gradient, along the electron transfer pathway ensures fast forward ET together with long lived radical ion pairs in close resemblance with natural photosynthesis. In simpler model systems other concepts for charge stabilization have been applied. In addition, it became evident in the course of this article that the spatial arrangement of the different building blocks in the photosynthetic model systems as well as the distance between the final electron donor and acceptor play key roles. In covalently linked conjugates the nature of the linkage determines the mechanism, the efficiency as well as the dynamics of ET. Charge transport can either occur through bond or through space, which is influenced by the design of the molecular spacer. Non-covalent systems, where electron donors and acceptors are self-assembled by various supramolecular binding motifs, i.e. π-π interactions, complimentary electrostatics or hydrogen bonding, facilitate the study of a wide range of systems via comparably easy preparation in close analogy to natural photosynthesis. The highest binding constants were realized in systems featuring cooperative binding motifs. Alternatively, electron donors and acceptors can also be brought together in mechanically interlocked systems, such as catenanes and rotaxanes. As seen for other systems, here also the distance between electron donor and acceptor, on one hand, and the rigidity of the system, on the other hand, is decisive for efficient transduction of energy as well as electrons.

Special attention is paid within this review on the role of fullerenes in photosynthetic model systems, due to their unique redox properties and low reorganization energy in ET reactions. While empty fullerenes function as excellent electron acceptors, EMFs exhibit amphoteric electronic properties. In addition to the mentioned advantages of empty fullerenes, their redox potentials can be finely tuned by the insertion of different metals or metal clusters into their interior. Consequently they function, depending on their endohedral composition either as electron donors, as electron acceptors or as both. Nevertheless, the properties of the attached chromophore have to match and the solvent environment has large impact as well. Besides the possibility of fine-tuning their redox characteristics via endohedral doping recent efforts place particular attention on exploring EMFs unique properties for artificial electron donor-acceptor systems. To this end, the stabilization of charges via stable open-shell electronic configurations, the reduction of orbital overlap for the charge recombination with enclosed frontier orbitals, and the impact of nuclear hyperfine interactions of the enclosed heavy atoms on the spin states and dynamics of radical ion pairs.

It was also highlighted that photocatalysts based on fullerenes can be expected to open new avenues in the fields of photo/chemical energy conversion and large-scale photocatalysis.

In summary it has been shown, that a wide range of possibilities is available to fine-tune and optimize the characteristics of artificial photosynthetic systems that efficiently harvest light, transfer energy as well as electrons generating long lived radical ion pair states.

4. Notes and references

1. J. Barber and P. D. Tran, *J. R. Soc. Interface*, 2013, **10**, 20120984-20120999.
2. R. E. Blankenship, D. M. Tiede, J. Barber, G. W. Brudvig, G. Fleming, M. Ghirardi, M. R. Gunner, W. Junge, D. M. Kramer, A. Melis, T. A. Moore, C. C. Moser, D. G. Nocera, A. J. Nozik, D. R. Ort, W. W. Parson, R. C. Prince and R. T. Sayre, *Science*, 2011, **332**, 805-809.
3. J. Barber, *Chem. Soc. Rev.*, 2009, **38**, 185-196.
4. S. Fukuzumi, K. Ohkubo and T. Suenobu, *Acc. Chem. Res.*, 2014, **47**, 1455-1464.
5. J. Messinger, W. Lubitz and J. R. Shen, *Phys. Chem. Chem. Phys.*, 2014, **16**, 11810-11811.
6. D. Gust, T. A. Moore and A. L. Moore, *Acc. Chem. Res.*, 2009, **42**, 1890-1898.
7. D. Gust and T. A. Moore, *Science*, 1989, **244**, 35-41.
8. C. C. Moser, C. C. Page and P. L. Dutton, in *Electron Transfer in Chemistry*, ed. V. Balzani, Wiley-VCH, Weinheim, 2001, vol. III, pp. 24-38.
9. S. Berardi, S. Drouet, L. Francas, C. Gimbert-Surinach, M. Guttentag, C. Richmond, T. Stoll and A. Llobet, *Chem. Soc. Rev.*, 2014, **43**, 7501-7519.
10. P. D. Frischmann, K. Mahata and F. Wurthner, *Chem. Soc. Rev.*, 2013, **42**, 1847-1870.
11. C. R. Nieto, J. Guilleme, C. Villegas, J. L. Delgado, D. Gonzalez-Rodriguez, N. Martin, T. Torres and D. M. Guldi, *J. Mater. Chem.*, 2011, **21**, 15914-15918.
12. Y. Rio, W. Seitz, A. Gouloumis, P. Vazquez, J. L. Sessler, D. M. Guldi and T. Torres, *Chem. Eur. J.*, 2010, **16**, 1929-1940.
13. W. Kaim, *Coord. Chem. Rev.*, 2011, **255**, 2503-2513.
14. B. Wardle, *Principles and Applications of Photochemistry*, John Wiley & Sons, Chichester, 2009.
15. M. Montalti, A. Credi, L. Prodi and M. T. Gandolfi, *Handbook of Photochemistry*, CRC Press, Boca Raton, 2006.
16. R. A. Marcus and N. Sutin, *Biochim. Biophys. Acta*, 1985, **811**, 265-322.
17. D. M. Guldi, *Chem. Soc. Rev.*, 2002, **31**, 22-36.
18. L. Feng, T. Akasaka and S. Nagase, in *Carbon Nanotubes and Related Structures*, eds. D. M. Guldi and N. Martín, Wiley-VCH, Weinheim, 2009.

19. A. A. Popov, S. Yang and L. Dunsch, *Chem. Rev.*, 2013, **113**, 5989-6113.
20. M. Rudolf, S. Wolfrum, D. M. Guldi, L. Feng, T. Tsuchiya, T. Akasaka and L. Echegoyen, *Chem. Eur. J.*, 2012, **18**, 5136-5148.
21. H. Shinohara, *Rep. Prog. Phys.*, 2000, **63**, 843-892.
22. H. Shinohara, in *Fullerenes: Chemistry, Physics, and Technology*, eds. K. M. Kadish and R. S. Ruoff, Wiley, New York, 2000, pp. 357-393.
23. S. Nagase, K. Kobayashi, T. Akasaka and T. Wakahara, in *Fullerenes: Chemistry, Physics, and Technology*, eds. K. M. Kadish and R. S. Ruoff, Wiley, New York, 2000, pp. 231-251.
24. *Endofullerenes: A New Family of Carbon Clusters*, Kluwer, Dordrecht, The Netherlands, 2002.
25. P. J. Bracher and D. I. Schuster, in *Fullerenes: From Synthesis to Optoelectronic Properties*, eds. D. M. Guldi and N. Martín, Kluwer Academic Publishers, Norwell, MA, 2002, pp. 163-202.
26. C. Luo, D. M. Guldi, H. Imahori, K. Tamaki and Y. Sakata, *J. Am. Chem. Soc.*, 2000, **122**, 6535-6551.
27. H. Imahori, D. M. Guldi, K. Tamaki, Y. Yoshida, C. Luo, Y. Sakata and S. Fukuzumi, *J. Am. Chem. Soc.*, 2001, **123**, 6617-6628.
28. D. M. Guldi, H. Imahori, K. Tamaki, Y. Kashiwagi, H. Yamada, Y. Sakata and S. Fukuzumi, *J. Phys. Chem. A*, 2004, **108**, 541-548.
29. B. Albinsson, M. P. Eng, K. Pettersson and M. U. Winters, *Phys. Chem. Chem. Phys.*, 2007, **9**, 5847-5864.
30. G. de la Torre, G. Bottari, M. Sekita, A. Hausmann, D. M. Guldi and T. Torres, *Chem. Soc. Rev.*, 2013, **42**, 8049-8105.
31. A. Hausmann, A. R. Soares, M. V. Martinez-Diaz, M. G. Neves, A. C. Tome, J. A. Cavaleiro, T. Torres and D. M. Guldi, *Photochem. Photobiol. Sci.*, 2010, **9**, 1027-1032.
32. A. R. Soares, M. V. Martinez-Diaz, A. Bruckner, A. M. Pereira, J. P. Tome, C. M. Alonso, M. A. Faustino, M. G. Neves, A. C. Tome, A. M. Silva, J. A. Cavaleiro, T. Torres and D. M. Guldi, *Org. Lett.*, 2007, **9**, 1557-1560.
33. R. Jacobs, K. Stranius, E. Maligaspe, H. Lemmetyinen, N. V. Tkachenko, M. E. Zandler and F. D'Souza, *Inorg. Chem.*, 2012, **51**, 3656-3665.
34. T. Lazarides, G. Charalambidis, A. Vuillamy, M. Reglier, E. Klontzas, G. Froudakis, S. Kuhri, D. M. Guldi and A. G. Coutsolelos, *Inorg. Chem.*, 2011, **50**, 8926-8936.
35. W. Seitz, A. J. Jimenez, E. Carbonell, B. Grimm, M. S. Rodriguez-Morgade, D. M. Guldi and T. Torres, *Chem. Commun.*, 2010, **46**, 127-129.
36. S. Kirner, M. Sekita and D. M. Guldi, *Adv. Mater.*, 2014, **26**, 1482-1493.
37. R. M. Williams, J. M. Zwier and J. W. Verhoeven, *J. Am. Chem. Soc.*, 1995, **117**, 4093-4099.
38. M. Prato, M. Maggini, C. Giacometti, G. Scorrano, G. Sandona and G. Farnia, *Tetrahedron*, 1996, **52**, 5221-5234.
39. D. M. Guldi, M. Maggini, G. Scorrano and M. Prato, *J. Am. Chem. Soc.*, 1997, **119**, 974-980.
40. N. Martin, L. Sanchez, M. A. Herranz, B. Illescas and D. M. Guldi, *Acc. Chem. Res.*, 2007, **40**, 1015-1024.
41. N. Martín, L. Sánchez, C. Seoane, R. Andreu, J. Garín and J. Orduna, *Tetrahedron Lett.*, 1996, **37**, 5979-5982.
42. N. Martín, F. Giacalone, J. L. Segura, N. Martín and D. M. Guldi, *Synth. Met.*, 2004, **147**, 57-61.
43. J.-F. Nierengarten, C. Schall and J.-F. Nicoud, *Angew. Chem. Int. Ed.*, 1998, **37**, 1934-1936.
44. D. Kuciauskas, P. A. Liddell, S. Lin, T. E. Johnson, S. J. Weghorn, J. S. Lindsey, A. L. Moore, T. A. Moore and D. Gust, *J. Am. Chem. Soc.*, 1999, **121**, 8604-8614.
45. N. Martín, L. Sánchez, B. Illescas and I. Pérez, *Chem. Rev.*, 1998, **98**, 2527-2548.
46. D. M. Guldi, *Chem. Soc. Rev.*, 2002, **31**, 22-36.
47. S. V. Kirner, D. Arteaga, C. Henkel, J. T. Margraf, N. Alegret, K. Ohkubo, B. Insuasty, A. Ortiz, N. Martín, L. Echegoyen, S. Fukuzumi, T. Clark and D. M. Guldi, *Chem. Sci.*, 2015, DOI: 10.1039/c5sc02051d.
48. K. Dürr, S. Fiedler, T. Linßen, A. Hirsch and M. Hanack, *Chem. Ber.*, 1997, **130**, 1375-1378.
49. T. G. Linssen, K. Dürr, M. Hanack and A. Hirsch, *J. Chem. Soc., Chem. Commun.*, 1995, 103.
50. T. Nojiri, M. M. Alam, H. Konami, A. Watanabe and O. Ito, *J. Phys. Chem. A*, 1997, **101**, 7943-7947.
51. Á. Sastre, A. Gouloumis, P. Vázquez, T. Torres, V. Doan, B. J. Schwartz, F. Wudl, L. Echegoyen and J. Rivera, *Org. Lett.*, 1999, **1**, 1807-1810.
52. D. M. Guldi, I. Zilbermann, A. Gouloumis, P. Vázquez and T. Torres, *J. Phys. Chem. B*, 2004, **108**, 18485-18494.
53. J. R. Pinzón, M. E. Plonska-Brzezinska, C. M. Cardona, A. J. Athans, S. S. Gayathri, D. M. Guldi, M. Á. Herranz, N. Martín, T. Torres and L. Echegoyen, *Angew. Chem. Int. Ed.*, 2008, **47**, 4173-4176.
54. J. R. Pinzón, M. E. Plonska-Brzezinska, C. M. Cardona, A. J. Athans, S. S. Gayathri, D. M. Guldi, M. Á. Herranz, N. Martín, T. Torres and L. Echegoyen, *Angew. Chem.*, 2008, **120**, 4241-4244.
55. J. R. Pinzón, C. M. Cardona, M. Á. Herranz, M. E. Plonska-Brzezinska, A. Palkar, A. J. Athans, N. Martín, A. Rodríguez-Fortea, J. M. Poblet, G. Bottari, T. Torres, S. S. Gayathri, D. M. Guldi and L. Echegoyen, *Chem. Eur. J.*, 2009, **15**, 864-877.
56. J. R. Pinzón, D. C. Gasca, S. G. Sankaranarayanan, G. Bottari, T. Torres, D. M. Guldi and L. Echegoyen, *J. Am. Chem. Soc.*, 2009, **131**, 7727-7734.
57. C. Schubert, M. Rudolf, D. M. Guldi, Y. Takano, N. Mizorogi, M. Á. Herranz, N. Martín, S. Nagase and T. Akasaka, *Phil. Trans. R. Soc. A*, 2013, **371**, 20120490-20120499.
58. K. Ohkubo, H. Kotani, J. Shao, Z. Ou, K. M. Kadish, G. Li, R. K. Pandey, M. Fujitsuka, O. Ito, H. Imahori and S. Fukuzumi, *Angew. Chem. Int. Ed.*, 2004, **43**, 853-856.
59. L. Feng, Z. Slanina, S. Sato, K. Yoza, T. Tsuchiya, N. Mizorogi, T. Akasaka, S. Nagase, N. Martín and D. M. Guldi, *Angew. Chem. Int. Ed.*, 2011, **50**, 5909-5912.
60. L. Feng, Z. Slanina, S. Sato, K. Yoza, T. Tsuchiya, N. Mizorogi, T. Akasaka, S. Nagase, N. Martín and D. M. Guldi, *Angew. Chem.*, 2011, **123**, 6031-6034.
61. B. Liu, H. Fang, X. Li, W. Cai, L. Bao, M. Rudolf, F. Plass, L. Fan, X. Lu and D. M. Guldi, *Chem. Eur. J.*, 2015, **21**, 746-752.
62. G. de la Torre, F. Giacalone, J. L. Segura, N. Martin and D. M. Guldi, *Chem. Eur. J.*, 2005, **11**, 1267-1280.
63. A. Lembo, P. Tagliatesta, D. M. Guldi, M. Wielopolski and M. Nuccetelli, *J. Phys. Chem. A*, 2009, **113**, 1779-1793.
64. M. Wielopolski, G. de Miguel Rojas, C. van der Pol, L. Brinkhaus, G. Katsukis, M. R. Bryce, T. Clark and D. M. Guldi, *ACS Nano*, 2010, **4**, 6449-6462.

65. S. Wolfrum, J. R. Pinzon, A. Molina-Ontoria, A. Gouloumis, N. Martin, L. Echegoyen and D. M. Guldi, *Chem. Commun.*, 2011, **47**, 2270-2272.
66. L. Sanchez, N. Martin and D. M. Guldi, *Angew. Chem. Int. Ed.*, 2005, **44**, 5374-5382.
67. K. Maurer, B. Grimm, F. Wessendorf, K. Hartnagel, D. M. Guldi and A. Hirsch, *Eur. J. Org. Chem.*, 2010, **2010**, 5010-5029.
68. B. Grimm, E. Karnas, M. Brettreich, K. Ohta, A. Hirsch, D. M. Guldi, T. Torres and J. L. Sessler, *J. Phys. Chem. B*, 2010, **114**, 14134-14139.
69. H. Isla, B. Grimm, E. M. Pérez, M. Rosario Torres, M. Ángeles Herranz, R. Viruela, J. Aragó, E. Ortí, D. M. Guldi and N. Martín, *Chem. Sci.*, 2012, **3**, 498-508.
70. I. Sanchez-Molina, B. Grimm, R. M. Krick Calderon, C. G. Claessens, D. M. Guldi and T. Torres, *J. Am. Chem. Soc.*, 2013, **135**, 10503-10511.
71. B. Grimm, J. Schornbaum, C. M. Cardona, J. D. van Paauwe, P. D. W. Boyd and D. M. Guldi, *Chem. Sci.*, 2011, **2**, 1530-1537.
72. A. J. Jimenez, B. Grimm, V. L. Gunderson, M. T. Vagnini, S. Krick Calderon, M. S. Rodriguez-Morgade, M. R. Wasielewski, D. M. Guldi and T. Torres, *Chem. Eur. J.*, 2011, **17**, 5024-5032.
73. N. Martin, *Chem. Commun.*, 2006, 2093-2104.
74. F. d'Souza and O. Ito, in *Handbook of Organic Electronics and Photonics* ed. H. S. Nalva, Wiley, 2008, vol. 1, pp. 485-521.
75. T. Tsuchiya, H. Kurihara, K. Sato, T. Wakahara, T. Akasaka, T. Shimizu, N. Kamigata, N. Mizorogi and S. Nagase, *Chem. Commun.*, 2006, 3585-3587.
76. T. Tsuchiya, K. Sato, H. Kurihara, T. Wakahara, T. Nakahodo, Y. Maeda, T. Akasaka, K. Ohkubo, S. Fukuzumi, T. Kato, N. Mizorogi, K. Kobayashi and S. Nagase, *J. Am. Chem. Soc.*, 2006, **128**, 6699-6703.
77. T. Tsuchiya, K. Sato, H. Kurihara, T. Wakahara, Y. Maeda, T. Akasaka, K. Ohkubo, S. Fukuzumi, T. Kato and S. Nagase, *J. Am. Chem. Soc.*, 2006, **128**, 14418-14419.
78. T. Tsuchiya, M. Wielopolski, N. Sakuma, N. Mizorogi, T. Akasaka, T. Kato, D. M. Guldi and S. Nagase, *J. Am. Chem. Soc.*, 2011, **133**, 13280-13283.
79. I. E. Kareev, E. Laukhina, V. P. Bubnov, V. M. Martynenko, V. Lloveras, J. Vidal-Gancedo, M. Mas-Torrent, J. Veciana and C. Rovira, *ChemPhysChem*, 2013, **14**, 1670-1675.
80. D. M. Guldi, J. Ramey, M. V. Martínez-Díaz, A. d. l. Escosura, T. Torres, T. Da Ros and M. Prato, *Chem. Commun.*, 2002, 2774-2775.
81. D. M. Guldi, A. Gouloumis, P. Vázquez and T. Torres, *Chem. Commun.*, 2002, 2056-2057.
82. T. Tsuchiya, M. Rudolf, S. Wolfrum, S. G. Radhakrishnan, R. Aoyama, Y. Yokosawa, A. Oshima, T. Akasaka, S. Nagase and D. M. Guldi, *Chem. Eur. J.*, 2013, **19**, 558-565.
83. T. Kato, *J. Mol. Struct.*, 2007, **838**, 84-88.
84. S.-i. Kobayashi, S. Mori, S. Iida, H. Ando, T. Takenobu, Y. Taguchi, A. Fujiwara, A. Taninaka, H. Shinohara and Y. Iwasa, *J. Am. Chem. Soc.*, 2003, **125**, 8116-8117.
85. L. Basurto, F. Amerikheirabadi, R. Zope and T. Baruah, *Phys. Chem. Chem. Phys.*, 2015, **17**, 5832-5839.
86. R. M. Calderon, J. Valero, B. Grimm, J. de Mendoza and D. M. Guldi, *J. Am. Chem. Soc.*, 2014, **136**, 11436-11443.
87. B. Grimm, J. Schornbaum, H. Jasch, O. Trukhina, F. Wessendorf, A. Hirsch, T. Torres and D. M. Guldi, *Proc. Natl. Acad. Sci. U.S.A.*, 2012, **109**, 15565-15571.
88. J. Santos, B. Grimm, B. M. Illescas, D. M. Guldi and N. Martin, *Chem. Commun.*, 2008, 5993-5995.
89. L. Moreira, J. Calbo, R. M. Krick Calderon, J. Santos, B. M. Illescas, J. Aragó, J.-F. Nierengarten, D. M. Guldi, E. Ortí and N. Martín, *Chem. Sci.*, 2015, **6**, 4426-4432.
90. V. Garg, G. Kodis, P. A. Liddell, Y. Terazono, T. A. Moore, A. L. Moore and D. Gust, *J. Phys. Chem. B*, 2013, **117**, 11299-11308.
91. G. Kodis, Y. Terazono, P. A. Liddell, J. Andreasson, V. Garg, M. Hambourger, T. A. Moore, A. L. Moore and D. Gust, *J. Am. Chem. Soc.*, 2006, **128**, 1818-1827.
92. P. K. Ghosh, A. Y. Smirnov and F. Nori, *J. Chem. Phys.*, 2011, **134**, 244103.
93. Y. Terazono, G. Kodis, P. A. Liddell, V. Garg, T. A. Moore, A. L. Moore and D. Gust, *J. Phys. Chem. B*, 2009, **113**, 7147-7155.
94. W. S. Li, K. S. Kim, D. L. Jiang, H. Tanaka, T. Kawai, J. H. Kwon, D. Kim and T. Aida, *J. Am. Chem. Soc.*, 2006, **128**, 10527-10532.
95. C. B. Kc, G. N. Lim and F. D'Souza, *Nanoscale*, 2015, **7**, 6813-6826.
96. D. M. Guldi, G. M. Rahman, V. Sgobba and C. Ehli, *Chem. Soc. Rev.*, 2006, **35**, 471-487.
97. V. Bandi, F. P. D'Souza, H. B. Gobeze and F. D'Souza, *Chem. Eur. J.*, 2015, **21**, 2669-2679.
98. V. Bandi, M. E. El-Khouly, K. Ohkubo, V. N. Nesterov, M. E. Zandler, S. Fukuzumi and F. D'Souza, *Chem. Eur. J.*, 2013, **19**, 7221-7230.
99. V. Bandi, H. B. Gobeze, V. N. Nesterov, P. A. Karr and F. D'Souza, *Phys. Chem. Chem. Phys.*, 2014, **16**, 25537-25547.
100. D. Gust, T. A. Moore and A. L. Moore, in *Electron Transfer in Chemistry*, ed. V. Balzani, Wiley-VCH, Weinheim, New York, Chichester, Brisbane, Singapore, Toronto, 2001, pp. 272-336.
101. M. Gilbert and B. Albinsson, *Chem. Soc. Rev.*, 2015, **44**, 845-862.
102. G. Bottari, G. de la Torre, D. M. Guldi and T. Torres, *Chem. Rev.*, 2010, **110**, 6768-6816.
103. K. Dirian, M. Á. Herranz, G. Katsukis, J. Malig, L. Rodríguez-Pérez, C. Romero-Nieto, V. Strauss, N. Martín and D. M. Guldi, *Chem. Sci.*, 2013, **4**, 4335.
104. S. Fukuzumi and K. Ohkubo, *Dalton Trans*, 2013, **42**, 15846-15858.
105. S. Fukuzumi, K. Ohkubo, F. D'Souza and J. L. Sessler, *Chem. Commun.*, 2012, **48**, 9801-9815.
106. D. M. Guldi and H. Imahori, *J. Porphyrins Phthalocyanines*, 2004, **08**, 976-983.
107. P. L. Anelli, P. R. Ashton, R. Ballardini, V. Balzani, M. Delgado, M. T. Gandolfi, T. T. Goodnow, A. E. Kaifer, D. Philp, P. Marek, L. Prodi, M. V. Reddington, A. M. Z. Slawin, N. Spencer, J. F. Stoddart, C. Vicent and D. J. Williams, *J. Am. Chem. Soc.*, 1992, **114**, 193-218.
108. P. R. Ashton, V. Balzani, A. Credi, O. Kocian, D. Pasini, L. Prodi, N. Spencer, J. F. Stoddart, M. S. Tolley, M. Venturi, A. J. P. White and D. J. Williams, *Chem. Eur. J.*, 1998, **4**, 590-607.
109. P. R. Ashton, T. T. Goodnow, A. E. Kaifer, M. V. Reddington, A. M. Z. Slawin, N. Spencer, J. F. Stoddart, C.

Vicent and D. J. Williams, *Angew. Chem. Int. Ed.*, 1989, **28**, 1396-1399.
110. J. D. Megiatto, Jr., D. I. Schuster, S. Abwandner, G. Miguel and D. M. Guldi, *J. Am. Chem. Soc.*, 2010, **132**, 3847-3861.
111. J. D. Megiatto, Jr., D. I. Schuster, G. d. Miguel, S. Wolfrum and D. M. Guldi, *Chem. Mater.*, 2012, **24**, 2472-2485.
112. J. D. Megiatto, Jr., R. Spencer and D. I. Schuster, *J. Mater. Chem.*, 2011, **21**, 1544.
113. K. Li, P. J. Bracher, D. M. Guldi, M. A. Herranz, L. Echegoyen and D. I. Schuster, *J. Am. Chem. Soc.*, 2004, **126**, 9156-9157.
114. K. Li, D. I. Schuster, D. M. Guldi, M. A. Herranz and L. Echegoyen, *J. Am. Chem. Soc.*, 2004, **126**, 3388-3389.
115. J. D. Megiatto, Jr., K. Li, D. I. Schuster, A. Palkar, M. A. Herranz, L. Echegoyen, S. Abwandner, G. Miguel and D. M. Guldi, *J. Phys. Chem. B*, 2010, **114**, 14408-14419.
116. J. D. Megiatto, Jr., R. Spencer and D. I. Schuster, *Org. Lett.*, 2009, **11**, 4152-4155.
117. D. I. Schuster, K. Li, D. M. Guldi and J. Ramey, *Org. Lett.*, 2004, **6**, 1919-1922.
118. L. Flamigni, A. M. Talarico, J. C. Chambron, V. Heitz, M. Linke, N. Fujita and J. P. Sauvage, *Chem. Eur. J.*, 2004, **10**, 2689-2699.
119. S. V. Kirner, D. M. Guldi, J. D. Megiatto, Jr. and D. I. Schuster, *Nanoscale*, 2015, **7**, 1145-1160.
120. S. V. Kirner, C. Henkel, D. M. Guldi, J. D. Megiatto Junior and D. I. Schuster, *Chem. Sci.*, 2015, DOI: 10.1039/c5sc02895g.
121. D. M. Guldi, L. Feng, S. G. Radhakrishnan, H. Nikawa, M. Yamada, N. Mizorogi, T. Tsuchiya, T. Akasaka, S. Nagase, M. Ángeles Herranz and N. Martín, *J. Am. Chem. Soc.*, 2010, **132**, 9078-9086.
122. L. Feng, S. Gayathri Radhakrishnan, N. Mizorogi, Z. Slanina, H. Nikawa, T. Tsuchiya, T. Akasaka, S. Nagase, N. Martín and D. M. Guldi, *J. Am. Chem. Soc.*, 2011, **133**, 7608-7618.
123. J. Messinger, *ChemSusChem*, 2009, **2**, 47-48.
124. F. Cataldo, S. Iglesias-Groth and A. Manchado, in *Fullerenes, Nanotubes and Carbon Nanostructures*, 2012, vol. 20, pp. 656-671.
125. C. Bruno, I. Doubitski, M. Marcaccio, F. Paolucci, D. Paolucci and A. Zaopo, *J. Am. Chem. Soc.*, 2003, **125**, 15738-15739.
126. C. A. Reed, *Science*, 2000, **289**, 101-104.
127. S. Fukuzumi, K. Ohkubo, H. Imahori and D. M. Guldi, *Chem. Eur. J.*, 2003, **9**, 1585-1593.
128. K. Ohkubo, R. Iwata, T. Yanagimoto and S. Fukuzumi, *Chem. Commun.*, 2007, 3139-3141.
129. L. Biczók and H. Linschitz, *J. Phys. Chem. A*, 2001, **105**, 11051-11056.
130. S. Fukuzumi, H. Mori, H. Imahori, T. Suenobu, Y. Araki, O. Ito and K. M. Kadish, *J. Am. Chem. Soc.*, 2001, **123**, 12458-12465.
131. K. Ohkubo, J. Ortiz, L. Martin-Gomis, F. Fernandez-Lazaro, A. Sastre-Santos and S. Fukuzumi, *Chem. Commun.*, 2007, 589-591.
132. M. Lederer, M. Rudolf, M. Wolf, D. M. Guldi, S. Zhao, X. Lu and L. Feng, in *Endohedral Metallofullerenes: Basics and Applications*, eds. X. Lu, L. Echegoyen, A. L. Balch, S. Nagase and T. Akasaka, CRC Press, Boca Raton, 2015, pp. 211-254.
133. Y. Takano, S. Obuchi, N. Mizorogi, R. García, M. Á. Herranz, M. Rudolf, D. M. Guldi, N. Martín, S. Nagase and T. Akasaka, *J. Am. Chem. Soc.*, 2012, **134**, 19401-19408.
134. L. Feng, M. Rudolf, S. Wolfrum, A. Troeger, Z. Slanina, T. Akasaka, S. Nagase, N. Martín, T. Ameri, C. J. Brabec and D. M. Guldi, *J. Am. Chem. Soc.*, 2012, **134**, 12190-12197.
135. M. Rudolf, L. Feng, Z. Slanina, T. Akasaka, S. Nagase and D. M. Guldi, *J. Am. Chem. Soc.*, 2013, **135**, 11165-11174.
136. L. Feng, M. Rudolf, O. Trukhina, Z. Slanina, F. Uhlik, X. Lu, T. Torres, D. M. Guldi and T. Akasaka, *Chem. Commun.*, 2015, **51**, 330-333.
137. M. Rudolf, O. Trukhina, J. Perles, L. Feng, T. Akasaka, T. Torres and D. M. Guldi, *Chem. Sci.*, 2015, **6**, 4141-4147.
138. Y. Kawashima, K. Ohkubo and S. Fukuzumi, *J. Phys. Chem. A*, 2013, **117**, 6737-6743.
139. S. Fukuzumi, H. Imahori, K. Okamoto, H. Yamada, M. Fujitsuka, O. Ito and D. M. Guldi, *J. Phys. Chem. A*, 2002, **106**, 1903-1908.
140. T. Abe, S. Tobinai, N. Taira, J. Chiba, T. Itoh and K. Nagai, *J. Phys. Chem. C*, 2011, **115**, 7701-7705.
141. T. Abe, J. Chiba, M. Ishidoya and K. Nagai, *RSC Adv.*, 2012, **2**, 7992-7996.
142. T. Abe, N. Taira, Y. Tanno, Y. Kikuchi and K. Nagai, *Chem. Commun.*, 2014, **50**, 1950-1952.